UNIVERSIDADE DA BEIRA INTERIOR
Ciências da Saúde

Development of graphene oxide based nanomaterials for cancer therapy

Ana Rita Lima Sousa

Dissertação para obtenção do Grau de Mestre em
Ciências Biomédicas
(2º ciclo de estudos)

Orientador: Professor Doutor Ilídio Joaquim Sobreira Correia
Co-orientador: Mestre Duarte Miguel de Melo Diogo

Covilhã, junho de 2018

“Success is walking from failure to failure with no loss of enthusiasm”

-Winston Churchill

Para a minha mãe, o meu pai e a minha irmã…

Acknowledgements

Primeiro, gostaria de agradecer ao meu orientador, o professor Ilídio Correia, por me conceder a enorme oportunidade de integrar o seu grupo de investigação. A sua orientação, conselhos e sugestões ao longo deste ano foram essenciais para a realização deste projeto. Agradeço também por mostrar um lado mais descontraído, que me surpreendeu.

Ao meu co-orientador, Duarte, agradeço por todo o apoio que me deu neste último ano, mesmo nas alturas em que a motivação faltava. Obrigada por ter sido a ponte para o desenvolvimento do meu pensar científico.

À minha parceira, a Cátia, obrigada por toda a ajuda que me deu. A constante troca de ideias e gargalhadas contribuiu muito para que este ano passasse tão rápido. À Cátia Sol, à Sofia e à Carolina obrigada por tornarem este último ano um pouquinho menos difícil de encarar. Nunca pensei que tão pouco tempo chegasse para construir uma amizade tão grande. Quero também agradecer aos restantes elementos do grupo do professor Ilídio pela boa disposição e ajuda ao longo do ano.

Para os meus amigos do coração, a família que a Covilhã me deu, agradeço todos os momentos passados. À Ana Luísa, em especial, agradeço todos os momentos de cumplicidade, todos os risos, todos os choros e todas as palavras de encorajamento. Tudo o que passámos juntas dava para escrever um livro! Nem a distância nos vai separar. À Rita, obrigada por me acolheres na tua vida, por aceitares os meus conselhos e por me fazeres ver que nas situações piores uma pessoa tem sempre que sorrir. À Cristiana, obrigada pelas suas constantes palhaçadas, que muitas vezes ajudaram a passar dias mais negativos.

À minha família, não há forma de expressar o quão grata estou por todos os esforços que fizeram e que tornaram possível esta minha jornada. À minha mãe, a voz da família, agradeço as palavras de encorajamento e compreensão que me transmite mesmo através de uma chamada de telemóvel. Ao meu pai, agradeço a sua confiança e cada piada sem sentido. À minha pequena irmã, que ao longo destes anos que estive longe vi crescer e tornar-se numa pessoa com garra e convicção, respondona e teimosa, agradeço por me fazeres ver que até as mais pequenas de nós conseguem chegar onde querem.

Por fim, para o meu Rui, um obrigado não chega para agradecer todo o apoio. Obrigada por partilhares comigo cada dia destes últimos 5 anos como se fosse o primeiro. Como sei que não somos bons com as palavras, deixo os gestos falarem por mim.

Resumo

O cancro da mama é uma das principais causas de morte em todo o mundo, afetando principalmente as mulheres. Os tratamentos mais comuns para esta doença incluem a radioterapia e a quimioterapia. No entanto, estas abordagens terapêuticas apresentam uma baixa eficácia e podem, também, induzir efeitos secundários adversos nos pacientes. Desta forma, existe uma enorme necessidade em desenvolver novos tratamentos mais eficazes para o cancro da mama.

Neste contexto, diferentes investigadores estão a desenvolver novas abordagens terapêuticas. Em particular, a terapia fototérmica mediada por nanomateriais tem recebido um interesse crescente por parte dos investigadores e profissionais de saúde. Esta abordagem tira partido das propriedades físico-químicas e óticas de alguns tipos de nanomateriais. Estas nanoestruturas responsivas à luz conseguem acumular-se preferencialmente na zona tumoral e posteriormente induzir, após irradiação com luz com um comprimento de onda na região do infravermelho próximo (NIR), um aumento de temperatura que pode danificar as células cancerígenas.

Nesta dissertação, materiais à base de óxido de grafeno reduzido (rGO) foram produzidos através de um método de redução ecológico e funcionalizados com um novo polímero anfifílico à base de ácido hialurónico (HA) para aplicação na terapia fototérmica do cancro da mama. O HA foi escolhido devido ao seu carácter hidrofílico e por possuir capacidade de direcionamento para os recetores CD44, que são sobreexpressos na membrana citoplasmática das células do cancro da mama. Os resultados obtidos revelaram que o tratamento do óxido de grafeno com ácido L-ascórbico (3 mM), durante 60 minutos, a 80 ºC, constituem as condições ideais de redução tendo em conta a absorção no NIR apresentada pelo rGO e a distribuição de tamanhos dos materiais obtidos. Posteriormente, a funcionalização do rGO com o polímero anfifílico à base de HA foi efetuada através de interações não-covalentes. A funcionalização melhorou a estabilidade, citocompatibilidade e internalização dos nanomateriais pelas células do cancro da mama que sobreexpressam o recetor CD44, o que confirma a capacidade de direcionamento desta nanoformulação. Adicionalmente, a terapia fototérmica mediada pelo rGO funcionalizado induziu a morte das células cancerígenas, confirmando assim o potencial desta nanoformulação para aplicação na terapia direcionada do cancro da mama.

Palavras-chave

Ácido hialurónico, Efeito fototérmico, Materiais 2D, Química ecológica, Terapia direcionada.

Resumo Alargado

Atualmente, o cancro é uma das principais causas de morte em todo o mundo. Em particular, o cancro da mama é o mais comum e o que tem uma maior taxa de mortalidade no sexo feminino. Este panorama deve-se à ineficácia das terapias convencionais (como a radioterapia e a quimioterapia) e aos elevados efeitos secundários que estas induzem nos pacientes. Deste modo é fundamental o desenvolvimento de novas modalidades terapêuticas para o cancro da mama.

Neste contexto, a terapia fototérmica (PTT) mediada por nanomateriais tem captado a atenção dos investigadores e profissionais de saúde. Este tipo de terapia tira partido das propriedades físico-químicas e óticas de alguns tipos de nanomateriais. Estas nanoestruturas, responsivas à luz, conseguem acumular-se preferencialmente na zona do tumor e induzir, após irradiação com luz, um aumento de temperatura que pode danificar as células. Nesta abordagem terapêutica, é de extrema importância utilizar luz com um comprimento de onda no infravermelho próximo (NIR; 750-1000 nm), uma vez que esta radiação não apresenta interações significativas com componentes biológicos, e possui uma elevada capacidade de penetração nos tecidos. Esta propriedade é fundamental para que a radiação alcance os nanomateriais que se acumulam no tumor. Assim, os nanomateriais concebidos para aplicação na PTT devem ter a capacidade de absorver na região do NIR.

De entre os diferentes nanomateriais responsivos à luz, o óxido de grafeno reduzido (rGO) tem demonstrado propriedades interessantes para aplicação na PTT do cancro devido à sua elevada absorção no NIR. No entanto, a utilização direta deste nanomaterial é limitada devido à sua i) baixa solubilidade em água ii) instabilidade coloidal, iii) baixa citocompatibilidade (devido à utilização de agentes tóxicos na sua produção) e iv) ausência de capacidade de direcionamento para as células cancerígenas.

Na presente dissertação, o rGO foi produzido através de um método ecológico e funcionalizado com um novo polímero anfifílico baseado em ácido hialurónico (HA) para aplicação na terapia fototérmica direcionada do cancro da mama. O HA foi selecionado tendo por base a sua hidrofilicidade e capacidade de ligação aos recetores CD44 que são sobreexpressos na membrana das células do cancro da mama. Estes recetores podem também ser encontrados na membrana citoplasmática das células saudáveis, porém encontram-se num estado quiescente (não se ligam ao HA). Por outro lado, o poli(anidrido maleico-*alt*-1-octadeceno) (PMAO) foi selecionado devido à sua hidrofobicidade e capacidade de adsorção na superfície do rGO. Assim, para produzir o polímero anfifílico, procedeu-se primeiramente à desacetilação do HA, de modo a poder-se conjugar os grupos amina deste aos grupos carboxilo do PMAO hidrolisado, através da química de carbodiimida.

Os resultados obtidos revelaram que o tratamento do óxido de grafeno com ácido L-ascórbico (3 mM), durante 60 minutos, a 80 ºC, constituem as condições ideais de redução. Assim, foi possível otimizar pela primeira vez a redução ecológica do óxido de grafeno tendo em conta a absorção no NIR e a distribuição de tamanhos dos materiais obtidos. Posteriormente, o rGO foi funcionalizado com o polímero anfifílico à base de HA através de interações não-covalentes. A funcionalização do rGO melhorou a sua estabilidade, citocompatibilidade e internalização pelas células do cancro da mama que sobreexpressam o recetor CD44, o que indica a capacidade de direcionamento desta nanoformulação. Para além disto, a terapia fototérmica mediada pelo rGO funcionalizado induziu a morte das células cancerígenas, confirmando assim o potencial desta nanoformulação para aplicação na terapia direcionada do cancro da mama.

Abstract

Breast cancer is one of the leading causes of death in the world, affecting mostly women. The most common treatments for this disease include radio- and chemo-therapies. However, these therapeutic approaches have a sub-optimal efficacy and can induce adverse side effects to patients. In this way, there is an urgent demand for the development of novel breast cancer treatments.

To improve the breast cancer treatment, researchers are developing new therapeutic approaches. In particular, photothermal therapy (PTT) mediated by nanomaterials has captured the attention of researchers and clinicians. This type of therapy takes advantage from the physicochemical and optical properties of some light-responsive nanostructures. These can accumulate preferentially in the tumor zone, and induce, after external irradiation with near infrared (NIR) light, a temperature increase that can damage cancer cells.

In this thesis, reduced graphene oxide (rGO) was produced by using an environmentally-friendly method. Then rGO was functionalized with a novel hyaluronic acid (HA)-based amphiphilic polymer to be applied in targeted breast cancer PTT. HA was selected due to its hydrophilic character and targeting capacity to the CD44 receptors, which are overexpressed on breast cancer cells' membrane. The obtained results revealed that the treatment of graphene oxide with L-ascorbic acid (3 mM) for 60 minutes at 80 °C is ideal considering the NIR absorption and the size distribution of the obtained materials. Then, rGO was functionalized with the HA-based amphiphilic polymer through non-covalent interactions. The functionalization of rGO improved its stability, cytocompatibility, and internalization by CD44 overexpressed by breast cancer cells, which indicates the targeting capacity of this nanoformulation. Furthermore, the on-demand PTT mediated by HA functionalized rGO induced cancer cells' death, thereby confirming the potential of this nanoformulation for targeted breast cancer therapy.

Keywords

2D materials, Green chemistry, Hyaluronan, Photothermal effect, Targeted therapy.

List of Publications

Articles published in international peer reviewed journals:

Alves, C. G.*, Lima-Sousa, R.*, de Melo-Diogo, D. *, Louro, R. O., Correia, I. J.; *IR780 based nanomaterials for cancer imaging and photothermal, photodynamic and combinatorial therapies*, International Journal of Pharmaceutics, 2018. 542 (1-2): p: 164-175. DOI: 10.1016/j.ijpharm.2018.03.020.

* These authors contributed equally to this article.

Articles submitted for publication in international peer reviewed journals:

Lima-Sousa, R., de Melo-Diogo, D., Alves, C. G., Costa, E. C., Louro, R. O., Correia, I. J., *Hyaluronic acid functionalized green reduced graphene oxide for targeted cancer photothermal therapy*. Under review.

de Melo-Diogo, D., Costa, E. C., Alves, C. G., Lima-Sousa, R., Louro, R. O., Correia, I. J., *POxylated Graphene Oxide Nanomaterials for Combination Chemo-phototherapy of Breast Cancer Cells*. Under review.

de Melo-Diogo, D., Lima-Sousa, R., Alves, C. G., Costa, E. C., Louro, R. O., Correia, I. J., *Functionalization of Graphene Family Nanomaterials for Application in Cancer Therapy*. Submitted for publication.

Alves, C. G., de Melo-Diogo, D., Lima-Sousa, R., Costa, E. C., Correia, I. J., *Hyaluronic acid functionalized micelles loaded with IR780 and DOX for targeted cancer chemo-photothermal therapy*. Under review.

Oral communications in scientific conferences

de Melo-Diogo, D., Pais-Silva, C., Costa, E. C., Alves, C. G., Lima-Sousa, R., Louro, R. O., Correia, I. J., *Near infrared light responsive nanomaterials for cancer therapy, XVI Portuguese Conference on Fracture*, Universidade da Beira Interior, 23th and 24th of April of 2018, Covilhã, Portugal.

de Melo-Diogo, D., Pais-Silva, C., Costa, E. C., Alves, C. G., Lima-Sousa, R., Louro, R. O., Correia, I. J., *Near infrared light responsive nanomaterials for cancer therapy*, *VI Jornadas de Bioengenharia*, Universidade da Beira Interior, 2nd and 3rd of May of 2018, Covilhã, Portugal.

Index

Figure Index

List of Abbreviations

ANOVA	Analysis of variance
CLSM	Confocal Laser Scanning Microscopy
DLS	Dynamic Light Scattering
DMEM-F12	Dulbecco's Modified Eagle's Medium F-12
DMSO	Dimethyl sulfoxide
DNA	Deoxyribonucleic acid
DSPE-PEG	1,2-distearoyl-*sn*-glycero-3-phosphoethanolamine-*N*-PEG
EDC	1-ethyl-3-(3-dimethylaminopropyl) carbodiimide
EPR	Enhanced Permeability and Retention
FBS	Fetal Bovine Serum
FTIR	Fourier Transform Infrared Spectroscopy
GO	Graphene oxide
HA	Hyaluronic acid
HA-*g*-PMAO	HA grafted PMAO
HA-rGO	HA-*g*-PMAO functionalized rGO
HH	Hydrazine hydrate
IC_{50}	Half maximal inhibitory concentration
LAA	L-ascorbic acid
MCF-7	Michigan Cancer Foundation-7
NIR	Near Infrared
NHDF	Normal Human Dermal Fibroblasts
NHS	*N*-Hydroxysuccinimide

PBS	Phosphate Buffer Saline
PEG	Poly(ethylene glycol)
PEG-*g*-PMAO	PEG-grafted poly(maleic anhydride-*alt*-1-octadecene)
PMAO	Poly(maleic anhydride-*alt*-1-octadecene)
PTT	Photothermal therapy
Rb	Retinoblastoma
rGO	Reduced graphene oxide
Rhod B	Rhodamine B
ROS	Reactive Oxygen Species
SD	Standard deviation
UV-Vis	Ultraviolet-visible
TEM	Transmission Electron Microscopy

Chapter 1

Introduction

1. Introduction

1.1. Cancer development, hallmarks, and treatments

1.1.1. Cancer

Cancer is one of the deadliest illnesses in the world, and its incidence is still high. It is estimated that by the end of 2018, more than 1,735,350 new cases of cancer will be diagnosed just in the United States of America [1]. In the same period and country, about 609,640 patients are estimated to die due to this disease [1]. In the case of Portugal, the National Health Service reported that in 2017, about 100 thousand citizens were receiving cancer treatment [2]. Furthermore, this disease is also growing at a rate of 3 % per year in this country [2].

Cancer is a disease characterized by an uncontrolled growth and proliferation of the cells (carcinogenesis) in response to genetic and epigenetic changes [3]. During this process, cells acquire new characteristics, that were termed by Hanahan and co-workers as the *cancer hallmarks* **(Figure 1)** [4-6]. These hallmarks comprise cancer cells capacity to: a) sustain chronic proliferation, b) evade tumor growth suppressors, c) resist death mechanism, d) have a limitless replicative immortality, e) induce uncontrollable angiogenesis, and f) activate a metastatic state [6].

Usually, cancer cells can produce the growth factors necessary for their proliferation (autocrine signaling) [6, 7]. Furthermore, cancer cells can also interact with the surrounding stroma, stimulating these cells to produce growth factors that promote cancer cells' proliferation [6, 7]. Additionally, the expression of growth factors receptors in the cancer cells' membrane is augmented, and these can induce an exaggerated intracellular response even if the levels of growth factors are low [6, 8]. Moreover, these malignant cells can bypass proliferation inhibitors (*e.g.* tumor suppressor protein 53 and Retinoblastoma (Rb) associated protein) by down-regulating tumor suppressor genes [6, 9, 10].

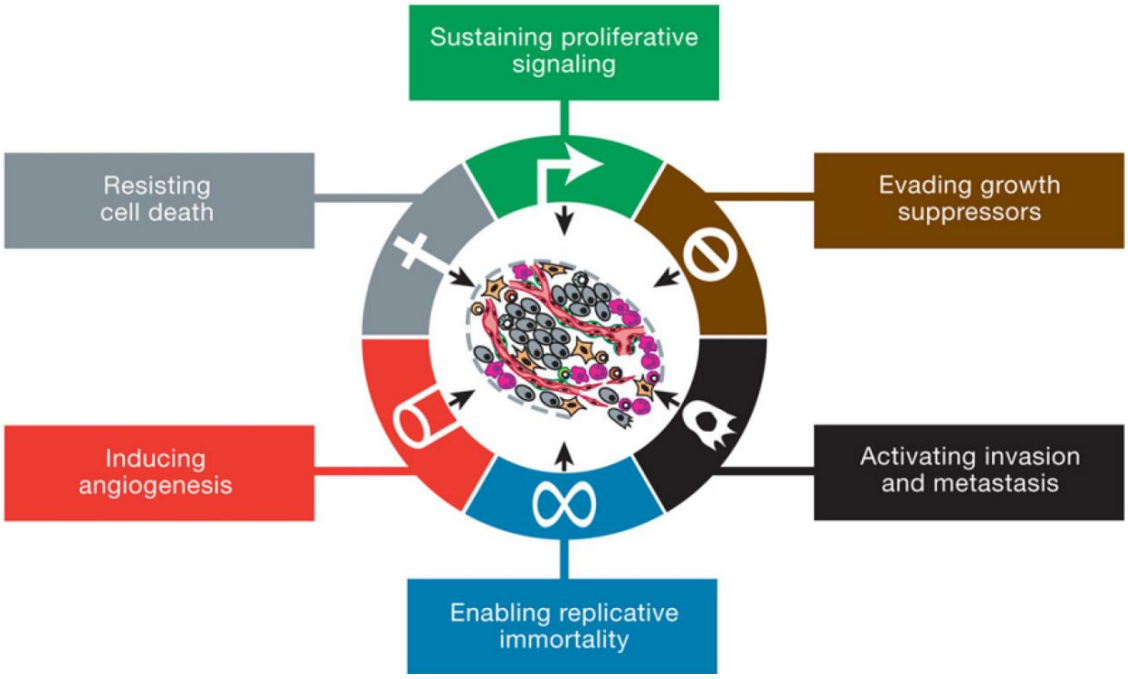

Figure 1: The six hallmarks of cancer described by Hanahan and Weinberg in 2000. These hallmarks comprise cancer cells' ability to i) sustain proliferative signaling through autocrine signaling and overexpression of growth factors' receptor on their membrane; ii) evade growth suppressors by down regulating their genes (*e.g.* RB and p53 proteins encoding genes); iii) activate an invasive and metastatic state through the regulation of the expression of cell migration-associated molecules (*e.g.* N-cadherin) and cell-cell adhesion proteins (*e.g.* E-cadherin); iv) have replicative immortality by overexpressing the telomerase; v) induce angiogenesis and vi) resist to programed death by regulating the expression of anti-apoptotic (*e.g.* Bcl-2, Bcl-x_L, and Bcl-w) and pro-apoptotic proteins (*e.g.* Bax and Bak). (Adapted from [6]).

Cancer cells can also resist to programmed death (apoptosis) [6]. To accomplish that, cancer cells up-regulate the expression of anti-apoptotic proteins (*e.g.* Bcl-2, Bcl-x_L, and Bcl-w*)* and down-regulate pro-apoptotic proteins (*e.g.* Bax and Bak) [6, 10, 11]. Malignant cells also overexpress telomerase [6], an enzyme that is responsible for the addition of telomeric segments at the ends of the chromosomes, conferring to them protection from degradation and/or end-to-end fusion [6]. This ultimately protects the cells from senescence and apoptosis, that would be triggered by the shortening of the chromosomes' ends [6, 12]. This mechanism gives to cancer cells a replicative immortality.

Cancer cells induce angiogenesis to meet their increased demand for oxygen, nutrients and to expel metabolites and carbon dioxide [6]. This switch in the vasculature from a quiescent state to a continuous growth state is essential for the growth of the tumor [6, 13]. Furthermore, cancer cells acquire the capacity to extravasate through the newly formed vasculature, that is abnormal in form and architecture [6]. Then, they form micro-metastasis in other tissues that subsequently originate larger tumors [6]. This escape is provoked by a down-regulation of the

expression of cell-to-cell adhesion proteins (*e.g.* E-cadherin) and up-regulation of cell migration associated molecules (*e.g.* N-cadherin) [6, 14].

In the recent years, the researchers' discoveries led to the introduction of two new cancer hallmarks: the capacity of cancer cells to reprogram their metabolism for better sustaining their proliferative state and the cancer cells' capacity to evade the immune system, specially lymphocytes T and B, macrophages, and natural killer cells [6]. Together, these mechanisms depict the complexity of cancer.

1.1.2. Breast cancer

Breast cancer is a heterogeneous disease that begins in the epithelial cells of the milk ducts [15]. This type of cancer is one of the most prevalent in women all over the world, representing 30 % of all the diagnosed cancers in this gender [1, 16]. It is estimated that 268,670 new cases will be identified in 2018 just in the USA [1]. In Portugal, this disease is also devastating. The *Liga Portuguesa Contra o Cancro* estimates that every year, 6,000 new cases of breast cancer are diagnosed and that 1,500 deaths will occur [17].

The main risk factors of breast cancer are the age (its incidence increases after the age of 50 years [1]), and genetic factors (strongly related to genetic mutations in the *BRCA 1* and *BRCA 2* genes) [18]. Furthermore, lifestyle options (*e.g.* diet, weight, alcohol intake and smoking) also strongly affect the progress of this disease [18].

In healthy breast tissues, the breast ducts are composed by several types of cells in a well-defined organization. The basement membrane is enclosed by myoepithelial cells and by a layer of luminal epithelial cells that is connected to the myoepithelial cells **(Figure 2)** [19]. The basement membrane is also surrounded by constituents of the stroma, namely fibroblasts, myofibroblasts, leucocytes and endothelial cells [19]. Cancer development starts when epigenetic and genetic alterations occur in all these cells [19]. These changes will induce i) a decrease in the number of myoepithelial cells, ii) the degradation of the basement membrane and iii) an increase in the stromal population [19], leading to the development of an *in situ* carcinoma **(Figure 2)**. This carcinoma transits to an invasive state when the myoepithelial cells and the basement membrane are completely depleted [7, 19]. Then, the tumor cells can evade the breast duct and colonize other tissues, leading to the appearance of metastasis **(Figure 2)**. Furthermore, tumor-associated macrophages are recruited to the tumor site to support breast cancer cells' invasive capacity and angiogenesis, thus facilitating cancer metastization [19, 20]. Additionally, carcinoma-associated fibroblasts secrete chemokines that induce cancer cells' migration and that also support angiogenesis [20]. These interactions contribute to the heterogenicity of breast cancer [20].

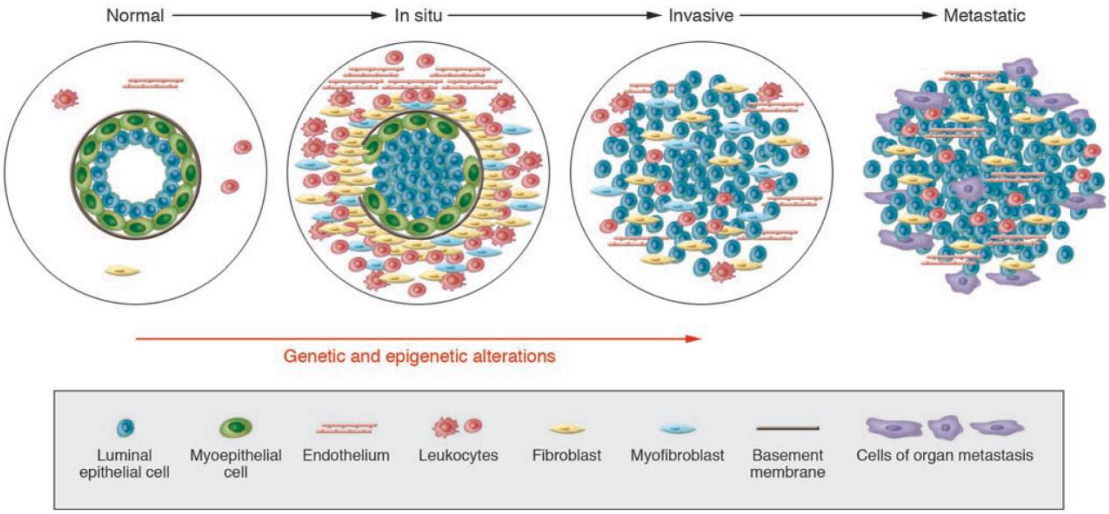

Figure 2: Schematic representation of the carcinogenesis process of breast cells. The appearance of breast cancer cells starts with the occurrence of genetic and epigenetic alterations in the cells of the breast duct. These will induce a reduction in the number of myoepithelial cells, the degradation of the basement membrane and an increase in the stromal population, thus forming an *in situ* carcinoma. The complete loss of the myoepithelial cells and the basement membrane will enable the establishment of an invasive carcinoma, which can originate metastasis. (Adapted from [19]).

The most common treatments for breast cancer are the surgical resection of the tumor (in early nonmetastatic stages), and radio- and chemo-therapies (in later stages of the development) [21, 22]. However, the therapeutic approaches for late-stage breast cancer have sub-optimal efficacy and induce severe side-effects, which can be threatening to patients' life [23]. Moreover, tumor cells may also develop resistance to radio- or chemo-therapies, further decreasing their therapeutic effectiveness [24]. In this way, it is urgent to develop novel and more effective breast cancer treatments to stop this devastating disease.

1.1.3. Photothermal therapy mediated by nanomaterials

Cancer photothermal therapy (PTT) mediated by nanomaterials has been showing promising results in cancer treatment [25]. This therapeutic approach takes advantage from the physicochemical and optical properties of nanomaterials [25]. These light-responsive nanomaterials, after intravenous administration, can extravasate from the tumor vasculature, through fenestrations (ranging from 200 to 1200 nm) leading to their accumulation in the tumor microenvironment. This accumulation of nanoparticles in the tumor occurs through the enhanced permeability and retention (EPR) effect [26] (**Figure 3**). Furthermore, these nanostructures remain accumulated within the tumor zone due to the impaired lymphatic drainage characteristic of tumor microenvironment [27, 28]. Afterwards, the nanomaterials are internalized by cancer cells, followed by external irradiation of the tumor site with laser light [25] (**Figure 3**).

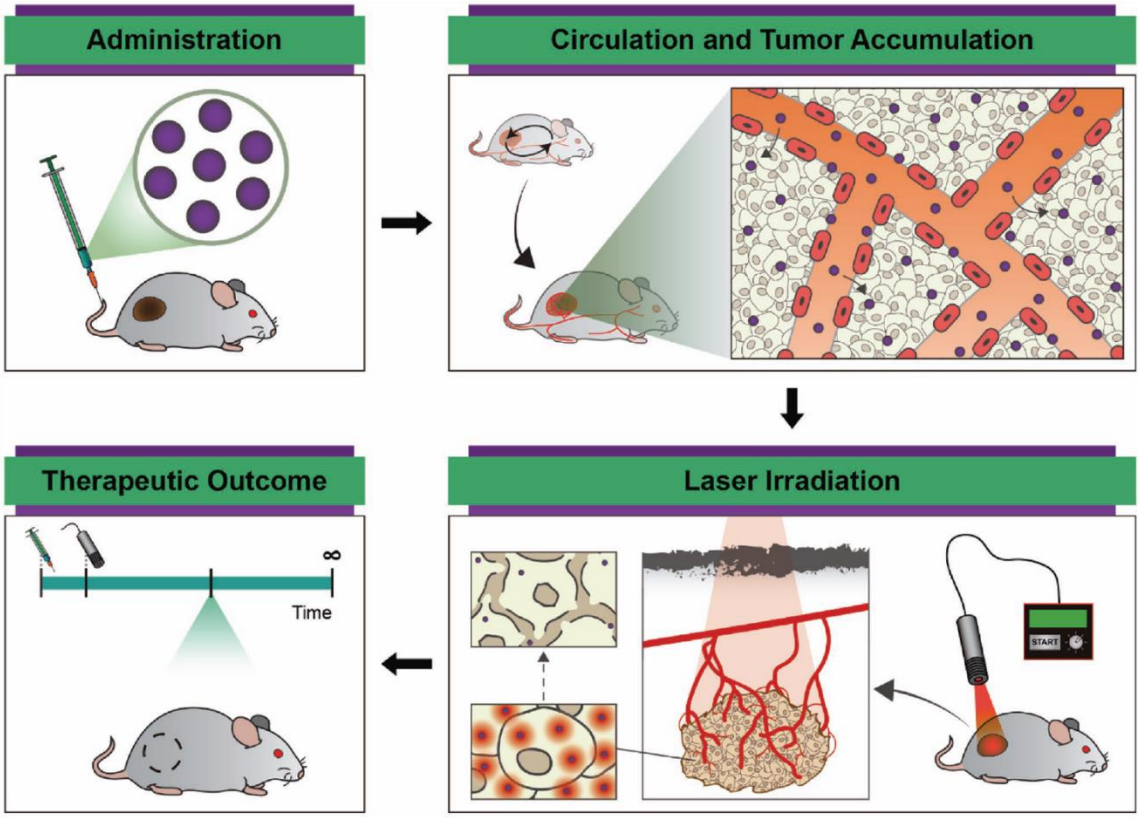

Figure 3: Representation of the various events occurring in PTT mediated by nanomaterials. Initially, the nanomaterials are administrated through intravenous administration and become accumulated in the tumor zone through the EPR effect. Subsequently, the tumor zone is irradiated with NIR laser light for a determined period of time and intensity. Then, the tumor homed-nanostructures absorb the NIR light energy and release it as heat. Finally, depending on the temperature variation attained, the ablation of mice's tumors can be achieved (Adapted from [25]).

The tumor zone is irradiated with near infrared light (NIR; 750-1000 nm) [29] due to its minimal interactions with biological components (*e.g.* water, hemoglobin, myoglobin or melanin) [29] **(Figure 4)**. This property guarantees that the NIR light achieves a deep penetration in the tissues (almost 2 cm) [30-32], which is fundamental for it to reach the tumor-homed nanostructures. Therefore, nanomaterials aimed to be applied in cancer PTT must display a high NIR absorption [29].

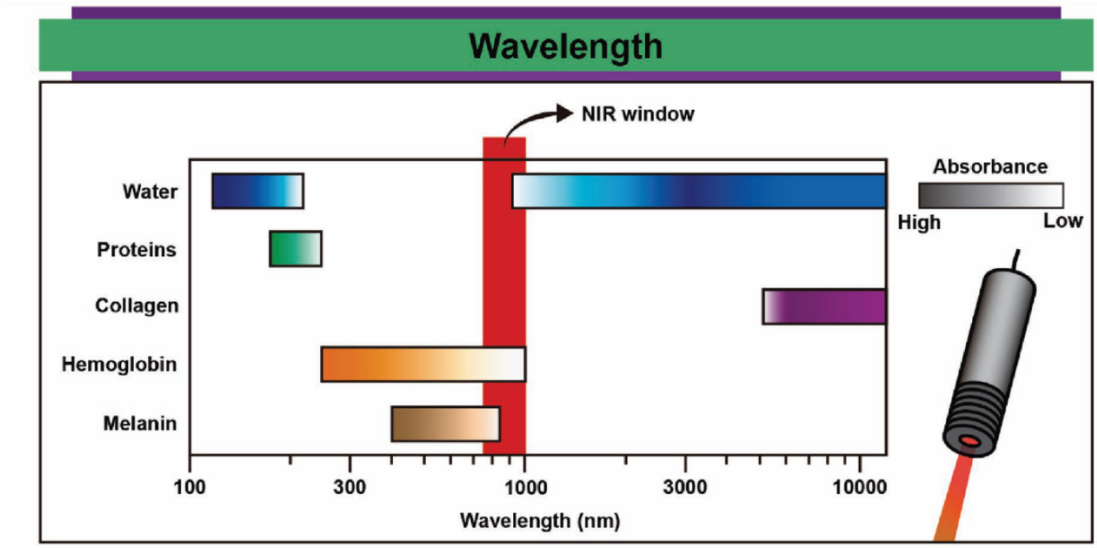

Figure 4: Schematic representation of the biological transparency window. The major constituents of the human body (water, proteins, collagen, hemoglobin, and melanin) have a minimal absorption between 750 and 1000 nm (NIR region). In this way, the use of NIR light in PTT ensures that the radiation achieves a high penetration depth and reaches the tumor homed-nanomaterials (Adapted from [25]).

Upon interaction with NIR light, the nanomaterials absorb its energy and convert it into heat [25]. This interaction can produce different therapeutic outcomes depending on the temperature variation attained. In general, in temperature increases to about 41 - 45 ºC, such variations can induce i) alterations on cells' metabolic functions; ii) inhibitions in the DNA repair mechanisms; iii) the formation of oxygen reactive species (ROS), and iv) sensitize cells to the action of other therapies [33-35]. In turn, hyperthermia to above 50 ºC can severely affect cells' functions (*e.g.* dysfunction of the enzymatic and mitochondrial functions, protein denaturation and membrane collapse [33]), and ultimately can lead to cells' necrosis [36].

So far, the most common nanomaterials used in cancer PTT are based on noble metal nanostructures (*e.g.* gold nanorods) [37]. Recently, researchers focused their attention in carbon-based nanomaterials for photothermal applications [38]. In fact, graphene oxide (GO) and its derivatives are one of the most recent NIR responsive nanomaterials explored in cancer PTT due to their high capacity to absorb NIR light and convert it into heat [39, 40].

1.2. Graphene oxide and reduced graphene oxide in cancer photothermal therapy

1.2.1. Graphene oxide and reduced graphene oxide

GO is a 2D graphitic material that is decorated with oxygen-containing functional groups on the base and edges of its aromatic structure (*e.g.* carboxyl, epoxy and hydroxyl groups) [41, 42]. This nanomaterial is generally obtained through the chemical oxidation of graphite and subsequent exfoliation of the graphite oxide, yielding GO **(Figure 5)**. Among all the synthesis methods used to obtain GO, the most usual are the Hummers' method and its improved version (also known as Tour method) [43].

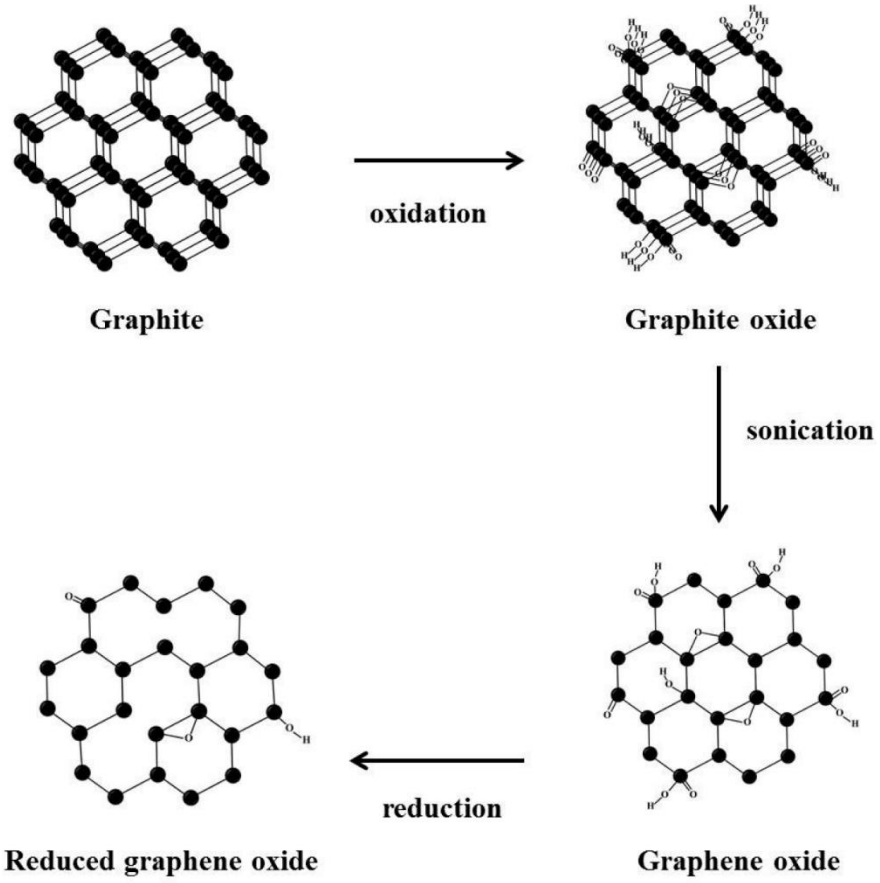

Figure 5: Schematic representation of the process used to produce reduced graphene oxide. First, graphite is chemically oxidized to graphite oxide. This material is then exfoliated, yielding GO. Subsequently, GO is treated with reducing agents (*e.g.* hydrazine hydrate), producing reduced GO (Adapted from [44]).

GO absorbs in the NIR region and thus can be employed as a photothermal agent [45]. Furthermore, the aromatic lattice of GO allows the loading of different compounds (*e.g.* chemotherapeutic drugs) on this nanomaterial through hydrophobic-hydrophobic interactions and π-π staking [42, 46]. Due to these two characteristics, GO is a promising agent for application in cancer chemo-photothermal therapy.

In order to further improve the therapeutic potential of GO, this material can be treated with reducing agents, yielding reduced graphene oxide (rGO) [47, 48]. For biomedical applications, the chemical treatment of GO with hydrazine hydrate (HH) is the most commonly applied route to synthesize rGO [48, 49]. The reduction recovers the graphitic structure of this nanomaterial by removing the oxygen functional groups [48]. Moreover, this modification greatly improves the NIR absorption and the hydrophobicity of this nanomaterial. In this way, when compared to GO, rGO has an improved photothermal and drug delivery capacities [40, 50, 51].

Despite its potential, rGO has some limitations that hinder its direct use in cancer therapy. rGO has a sub-optimal biocompatibility, mostly related to the HH used in the reduction process, which is a highly hazardous reagent [40]. To overcome this limitation, new environmentally-friendly methods aimed to reduce GO are under investigation. In this regard, L-ascorbic acid (LAA), or Vitamin C, has been successfully employed in the reduction of GO [52, 53]. In fact, this molecule can render rGO more cytocompatible than that attained using HH [52, 53]. However, the LAA-mediated reduction of GO is not yet optimized considering the NIR absorption and the nanometric size distribution of the obtained nanostructure, which are crucial features for the application of rGO in cancer PTT.

Furthermore, rGO has a low water solubility, and becomes precipitated in biological fluids, thus displaying a low colloidal stability [48, 50]. Moreover, the surface of rGO can adsorb proteins during circulation and these nanomaterials can also be internalized by macrophages [54, 55]. These events induce the clearance of rGO, thus diminishing its ability to reach the tumor zone by taking advantage from the EPR effect. Furthermore, rGO is not tailored to become selectively internalized by cancer cells [56] and thus cannot mediate a cancer cell-selective therapeutic effect upon laser irradiation. These problems can be mitigated by functionalizing rGO with amphiphilic polymers, enabling its successful application in cancer therapy.

1.2.2. Functionalization of reduced graphene oxide with amphiphilic polymers

The problems associated with the use of rGO in cancer therapy can be surpassed through the functionalization of this nanomaterial with amphiphilic polymers through non-covalent interactions. In this process, the hydrophobic blocks of the amphiphilic polymer become adsorbed to the aromatic matrix of rGO, while the hydrophilic segments become projected into the aqueous medium (**Figure 6**).

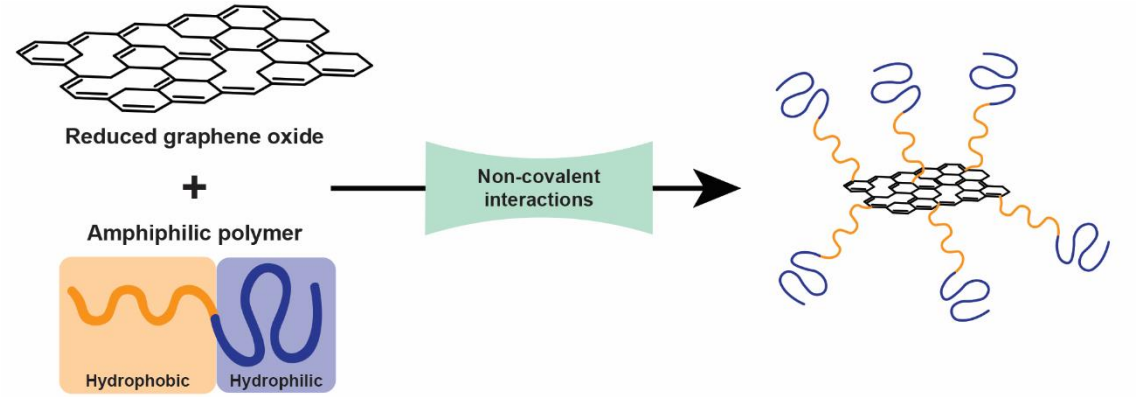

Figure 6: Schematic representation of the functionalization of rGO with amphiphilic polymers through non-covalent interactions (hydrophobic-hydrophobic interactions).

In this regard, the functionalization of rGO with Poly(ethylene glycol) (PEG)-based amphiphilic polymers has been the most studied approach [50, 57, 58]. For instance, the functionalization of rGO with PEG grafted poly(maleic anhydride-*alt*-1-octadecene) (PEG-*g*-PMAO) improves the solubility and stability of this nanomaterial, allowing its administration to tumor-bearing mice [57]. Furthermore, rGO functionalized with PEG-*g*-PMAO also displays an excellent biocompatibility both *in vitro* and *in vivo* [57]. PEG-based amphiphilic coatings can also reduce nanomaterials' opsonization and recognition by immune system cells [59, 60]. In this way, coating rGO with PEG-*g*-PMAO improves nanomaterials' blood circulation time, and consequently, their ability to accumulate in the tumor through the EPR effect [50].

Taking into account that PEG-*g*-PMAO is not commercially available, 1,2-distearoyl-*sn*-glycero-3-phosphoethanolamine-*N*-PEG (DSPE-PEG) has also been explored in the functionalization of rGO [61]. In fact, DSPE-PEG coatings can also improve the hydrophilicity, colloidal stability, and biocompatibility of rGO [61]. However, DSPE-PEG coated nanomaterials display a lower blood circulation time than those coated with PEG-*g*-PMAO, and therefore achieve a lower tumor uptake [40, 61].

Besides PEG-based amphiphilic polymers, Dextran- and Albumin-based coatings can also improve the colloidal stability, biocompatibility and tumor uptake of rGO [57, 62]. However, the PEG-, Dextran- and Albumin-based coatings do not display targeting capacity towards cancer cells. In this way, rGO functionalized with these amphiphilic materials can affect, upon NIR laser irradiation, both the cancer and the healthy cells found within the tumor microenvironment. Therefore, engineering amphiphilic polymers with targeting capacity is of uttermost importance.

1.2.3 Engineering amphiphilic polymers with targeting capacity

The functionalization of rGO with amphiphilic polymers with targeting capacity can further improve the therapeutic potential of this nanomaterial. This modification can address the critical problems of rGO (solubility, stability, and biocompatibility) and also ensures that the nanomaterials are specifically internalized by cancer cells [61]. In this way, rGO functionalized with amphiphilic polymers with targeting capacity may allow a cancer cell-selective PTT.

However, the amphiphilic polymers commonly explored in the functionalization of rGO do not have targeting capacity. Furthermore, developing amphiphilic materials that contain ligands that bind to the overexpressed receptors found on cancer cells' membrane can be complex and laborious to obtain. In fact, engineering such materials often requires the use of heterofunctional hydrophilic polymers. In this process, one of the functional groups is conjugated to the targeting ligand (*e.g.* folic acid, transferrin) [63, 64], while the other group attaches to the hydrophobic block, leading to the assembly of an amphiphilic polymer modified with a targeting ligand.

Herein, we hypothesized to use hyaluronic acid (HA) in the formulation of targeted-amphiphilic polymers. HA is a hydrophilic, biocompatible and biodegradable polysaccharide [65] that can bind to the CD44 receptors [66, 67], which are overexpressed on the membrane of several types of cancer cells, including breast cancer cells [67-69]. Additionally, normal cells express the CD44 receptors in a quiescent state, which do not display a binding capacity to HA [67]. This property further demonstrates the potential of using HA in targeted therapies.

Considering that poly(maleic anhydride-*alt*-1-octadecene) (PMAO) can efficiently adsorb to rGO surface [70], the conjugation of this hydrophobic polymer with HA seems to be a promising approach to obtain HA-based amphiphilic polymers (**Figure 7**). However, HA does not have active conjugation sites compatible with its conjugation to PMAO. In this way, a convenient route to synthesize this HA-based amphiphilic material could be using the carbodiimide chemistry to conjugate the amine-groups of deacetylated HA to the carboxyl-groups of hydrolyzed PMAO (**Figure 7**).

Overall, employing this novel HA-based amphiphilic polymer in the functionalization of environmentally-friendly reduced GO appears to be a promising strategy to produce nanomaterials with improved cytocompatibility and that may be able to mediate a photothermal effect selective to breast cancer cells.

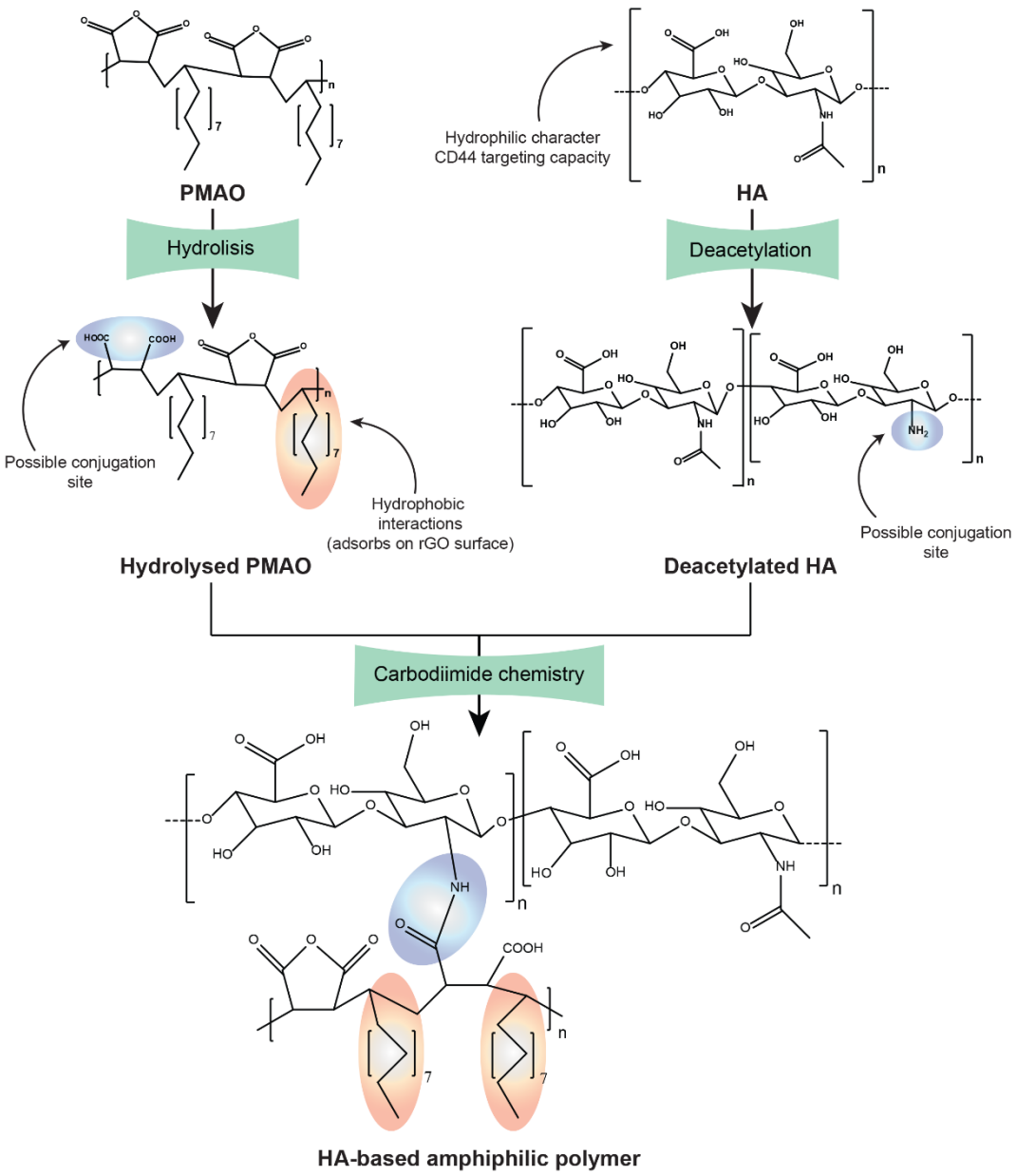

Figure 7: Schematic representation of the possible route used for synthesizing the HA-based amphiphilic polymer. First, PMAO must be hydrolyzed (opening of the anhydride rings) and HA must be deacetylated (acetyl-groups removal). These modifications yield carboxylic groups in PMAO and amine groups in HA. These functional groups can be conjugated through the carbodiimide chemistry, thus rendering the HA-based amphiphilic polymer.

Aims

The aim of this dissertation work plan was to functionalize rGO with a novel HA-based amphiphilic polymer for application in targeted breast cancer PTT.

The specific aims of this dissertation are:

- Optimization of the protocol to perform an environmentally-friendly reduction of GO;
- Production and characterization of the HA-based amphiphilic polymer;
- Functionalization of the rGO with the HA-based amphiphilic polymer;
- Characterization of the physicochemical, optical and photothermal properties of the HA-functionalized rGO;
- Evaluation of the cytocompatibility of the rGO and HA-functionalized rGO;
- Investigation of the targeting capacity of the HA-functionalized rGO towards cancer cells;
- Evaluation of the PTT mediated HA-functionalized rGO on breast cancer cells.

Chapter 2

Experimental Section

2. Experimental Section

2.1. Materials

Dimethyl Sulfoxide (DMSO) and LAA were purchased from Fisher Scientific (Oeiras, Portugal). Dulbecco's Modified Eagle's Medium F-12 (DMEM-F12), GO nanocolloids, *N*-Hydroxysuccinimide (NHS), Paraformaldehyde, PMAO (30000-50000 Da), penicillin/streptomycin and resazurin were acquired from Sigma–Aldrich (Sintra, Portugal). HA sodium salt (8000-15000 Da) was obtained from Carbosynth (Berkshire, United Kingdom). 1-ethyl-3-(3-dimethylaminopropyl) carbodiimide (EDC) was obtained from Merck (Darmstadt, Germany). Michigan Cancer Foundation-7 (MCF-7) cell line was gotten from ATCC (Middlesex, United Kingdom). Normal Human Dermal Fibroblasts (NHDF) were brought from Promo-Cell (Heidelberg, Germany). Fetal Bovine Serum (FBS) was purchased from Biochrom AG (Berlin, Germany). Water used in all experiments was double deionized (0.22 μm filtered 18.2 MΩ cm).

2.2. Methods

2.2.1. Optimization of the green reduction of GO

The optimization of the environmentally-friendly reduction of GO was performed by adapting a method previously described [71]. Briefly, GO was sonicated (Branson 5800, Branson Ultrasonics, CT, USA) for 6 h before its use. Then, 1 mL of GO (200 μg/mL) and LAA (3 mM or 1.5 mM) were reacted at 80 °C during 30, 45, 60, 90 or 120 min. Afterwards, the reduction process was stopped by cooling the samples in an ice-water bath.

2.2.2. Functionalization of rGO with HA-*g*-PMAO

To perform the functionalization of GO, this material (200 μg/mL, 1 mL) was mixed with 500 μg of HA-*g*-PMAO (which was synthesized as described in Appendix 6.1-6.3) and sonicated for 60 min. Afterward, this solution was dialyzed against water (14 kDa cut-off dialysis membrane) for 90 min to remove LAA and centrifuged to remove any aggregates. The supernatant was then recovered, yielding HA-*g*-PMAO functionalized rGO.

2.2.3. Characterization of rGO and HA-rGO based materials

The efficiency of the reduction of GO was monitored by UV-Vis spectroscopy using an Evolution 201 spectrophotometer (Thermo Scientific Inc., MA, USA), over the wavelength range from 200 to 1000 nm, and by Dynamic Light Scattering (DLS) in a Zetasizer Nano ZS (Malvern Instruments Ltd., Worcestershire, UK), at a scattering angle of 173°. The successful functionalization of rGO with HA-*g*-PMAO was confirmed through Fourier Transform Infrared Spectroscopy (FTIR)

using a Nicolet iS10 spectrometer (Thermo Scientific Inc., MA, USA), DLS and UV-Vis spectroscopy. Furthermore, HA-rGO nanosized dimensions were determined by Transmission Electron Microscopy (TEM), using a HT7700 microscope (Hitachi, Japan), operated at an accelerating voltage of 100 kV. For this purpose, samples were stained with phosphotungstic acid (2 % (w/v)). The photothermal capacity of HA-rGO was assessed by irradiating samples with NIR radiation (808 nm, 1.7 W/m^2) over a period of 5 min, and the temperature changes were monitored with a thermocouple thermometer.

2.2.4. Evaluation of the cytocompatibility of rGO and HA-rGO

The cytotoxic profile of rGO and HA-rGO was characterized using MCF-7 and NHDF as model cells [72]. In brief, 1 x 10^4 cells/well were seeded in 96-well plates with DMEM-F12 medium supplemented with 10 % FBS and 1 % of penicillin/streptomycin, at 37 ºC, in an incubator with a humidified atmosphere containing 5 % CO_2. After 24 h, the medium was replaced by fresh cell culture medium containing rGO or HA-rGO at different concentrations and then cells were incubated for 24 and/or 48 h. After this period, the medium was replaced with fresh cell culture medium containing resazurin (10 % (v/v)) and cells were incubated for 4 h in the dark (37 ºC, 5 % CO_2). Cells' viability was then assessed by analyzing the fluorescence of resorufin (λ_{ex} = 560 nm; λ_{em} = 590 nm) with a Spectramax Gemini EM spectrofluorometer (Molecular Devices LLC, CA, USA). Cells solely incubated with culture medium (without rGO derivatives) or treated with ethanol (70 % (v/v)) were used as negative (K-) and positive (K+) control, respectively.

2.2.5. Investigation of the targeting capacity of HA-rGO

To evaluate HA-rGO cellular uptake, this nanomaterial was labelled with Rhodamine B (Rhod B) as previously described elsewhere [47]. In brief, HA-rGO (200 µg/mL, 1 mL) was sonicated with Rhod B for 30 minutes. Afterwards, the solution was dialyzed against water for 90 min (1000 Da cut-off dialysis membrane) to remove the non-bounded Rhod B and centrifuged to remove any bigger aggregates.

To confirm the targeting capacity of HA-rGO to CD44 overexpressing cancer cells, the uptake of Rhod B labelled HA-rGO by MCF-7 cells (overexpressing CD44) [73, 74] and NHDF (that do not overexpress CD44) [75] was analyzed by Confocal Laser Scanning Microscopy (CLSM). Briefly, µ-slide 8-well imaging plates (Ibidi GmbH, Munich, Germany) were seeded with 1.5 x 10^4 cells/well and after 48 h, cells were incubated with cell culture medium containing Rhod B labelled HA-rGO (68.7 µg/mL of Rhod B equivalents) or free Rhod B (68.7 µg/mL) during 4 h. Subsequently, cells were fixed with paraformaldehyde 4 % for 15 min and then rinsed with a phosphate buffered saline (PBS) solution. Zeiss LSM 710 confocal microscope (Carl Zeiss AG, Oberkochen, Germany) was used for imaging experiments (λ_{ex} = 514 nm; λ_{em} = 513-703 nm). Non-treated cells and cells incubated with free-Rhod B were used as controls.

2.2.6. *In vitro* evaluation of the phototherapeutic effect mediated by HA-rGO

The photothermal effect mediated by HA-rGO was evaluated by using a previously described protocol [38]. In brief, MCF-7 cells at a density of 1 x 10^4 cells/well were seeded in 96-well plates with DMEM-F12 culture medium and after 24 h, the medium was replaced by fresh medium containing different concentrations of HA-rGO (25, 50 and 75 μg/mL). After 4 h, cells were irradiated with NIR light (808 nm, 1.7 W/cm^2, 5 min). After 24 h of incubation, cells' viability was determined through the resazurin assay as described above.

2.2.7. Statistical analysis

One-way ANOVA analysis with Student–Newman–Keuls test was used for multiple groups comparison. A p-value lower than 0.05 ($*p < 0.05$) was considered statistically significant. For data analysis, GraphPad Prism v6.0 (Trial version, GraphPad Software, CA, USA) was used.

Chapter 3

Results and Discussion

3. Results and Discussion

3.1. Optimization of the environmentally-friendly reduction of GO

The application of reduced forms of GO in cancer therapy is appealing since these materials have a higher NIR absorption than GO, resulting in an improved photothermal capacity [40]. However, rGO is usually obtained by treating GO with HH, which is a highly hazardous reducing agent [76]. In order to avoid such drawbacks, herein an environmentally-friendly method was used to perform the reduction of GO [52, 53, 71, 77]. To achieve that, LAA solutions (1.5 and 3 mM) were added to GO and then incubated at 80 ºC for various periods (**Figure 8**).

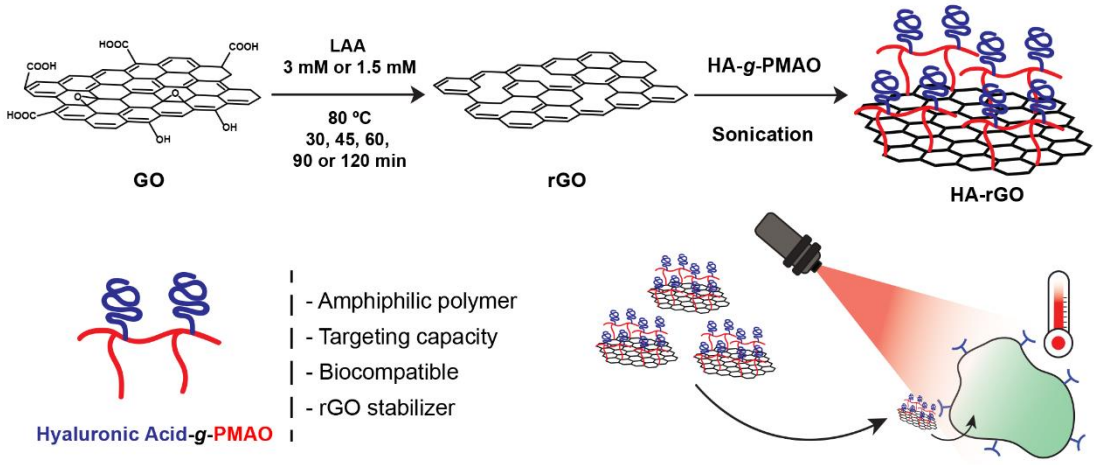

Figure 8: Schematic representation of the reduction and functionalization of rGO with HA-*g*-PMAO and its application in cancer photothermal therapy

Overall, by increasing the LAA concentration and the reaction time, a darkening of the GO solution and an increase on materials' NIR absorption were attained (**Figure 9C and D**). Nevertheless, the size distribution of the materials remained unaffected for the conditions tested (**Figure 9A and B**). This is of uttermost importance since the reduction of GO greatly reduces its solubility and could have increased the nanomaterials' size through agglomeration. Therefore, rGO obtained by using 3 mM of LAA and 60 min of reaction time was selected for the subsequent assays since it presented a good balance between NIR absorption and preparation time.

In comparison to a previous study where LAA was used to reduce GO [77], in this study we used a lower concentration of LAA (3 *vs*. 5.7 mM) and a shorter reaction time (1 *vs*. 12-48 h). Such results attest the convenience of the optimized green reduction method.

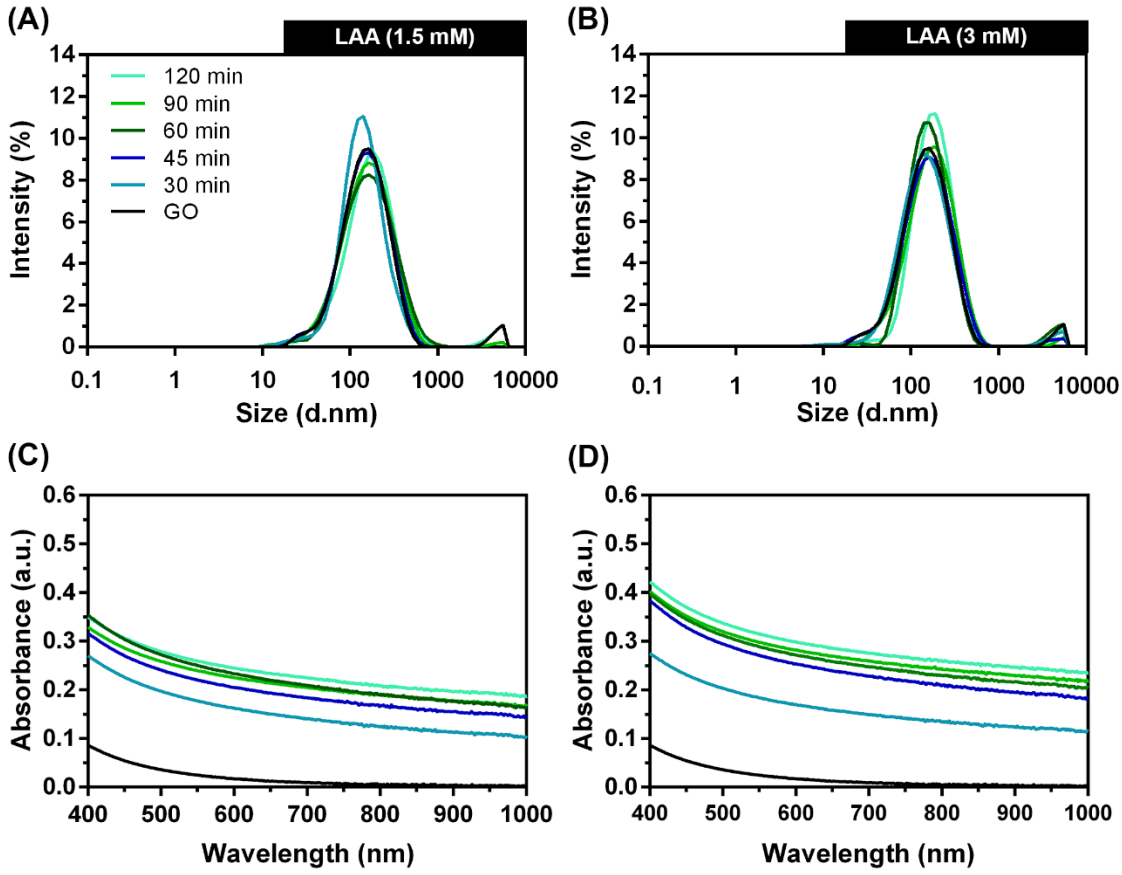

Figure 9: DLS size distribution and Vis-NIR absorption spectra of GO and rGO. DLS size distribution of GO (25 µg/ml) and rGO (25 µg/ml) at different times of reduction (A-B); Vis-NIR absorption spectra of GO (25 µg/ml) and rGO (25 µg/ml) at different times of reduction (C-D). (A) and (C) refer to GO reduced with 1.5 mM LAA. (B) and (D) refer to GO reduced with 3 mM LAA.

3.2. Functionalization of rGO with HA-*g*-PMAO

A simple sonication method was used to functionalize rGO with HA-*g*-PMAO (the characterization of HA-*g*-PMAO is reported in Appendix; **Figure 17-19**). In this process, the hydrophobic alkyl tail of HA-*g*-PMAO binds to the aromatic lattice of rGO through non-covalent interactions (hydrophobic-hydrophobic interactions). Moreover, the HA segments form a hydrophilic corona, which confer stability and cancer cell targeting capacity to this nanoformulation (**Figure 8**).

The successful functionalization of rGO with HA-*g*-PMAO was confirmed through FTIR analysis (**Figure 10A**). Before functionalization, rGO displays a peak at 1614 cm^{-1} (C=C stretch) and one with a low intensity at 1737 cm^{-1} (C=O stretch), which also confirm the restoration of the graphitic matrix of this material upon reduction. Furthermore, the peak at 3258 cm^{-1} (O-H stretch) suggests that some LAA traces are still present in rGO. On the other hand, the FTIR spectrum of HA-rGO presents peaks at 2919 cm^{-1} (C-H stretch) and 1730 cm^{-1} (C=O stretch),

which belong to the alkyl and ketone/carboxyl groups of HA-*g*-PMAO, respectively, thus confirming the successful preparation of HA-rGO. The DLS analysis demonstrated that the functionalization of rGO with HA-*g*-PMAO did not impact on its size distribution (**Figure 10B**). In fact, when compared to rGO, HA-rGO presents a monomodal size distribution, which suggests that the HA-based coating can improve the stability of the nanostructures.

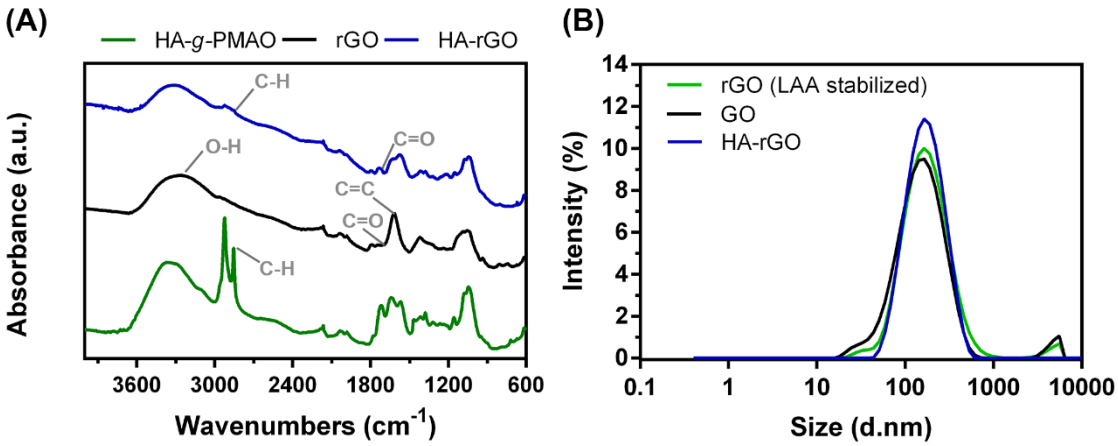

Figure 10: Characterization of HA-rGO. FTIR spectra of rGO, HA-*g*-PMAO, and HA-rGO (A); DLS size distribution of GO, rGO (LAA stabilized) and HA-rGO (B).

The nanosized dimensions of HA-rGO were then confirmed by TEM (**Figure 11**), revealing that these materials have an average lateral size of 108 ± 51 nm. These values are within the optimal range for passive tumor accumulation through the EPR effect [27]. The zeta potential of HA-rGO was determined to be slightly more negative than that of rGO (LAA stabilized) (HA-rGO: -28.6 ± 1.0 mV; rGO: -26.9 ± 0.3 mV). Nevertheless, the surface charge of HA-rGO is in line with that reported for other HA-based materials [78-80].

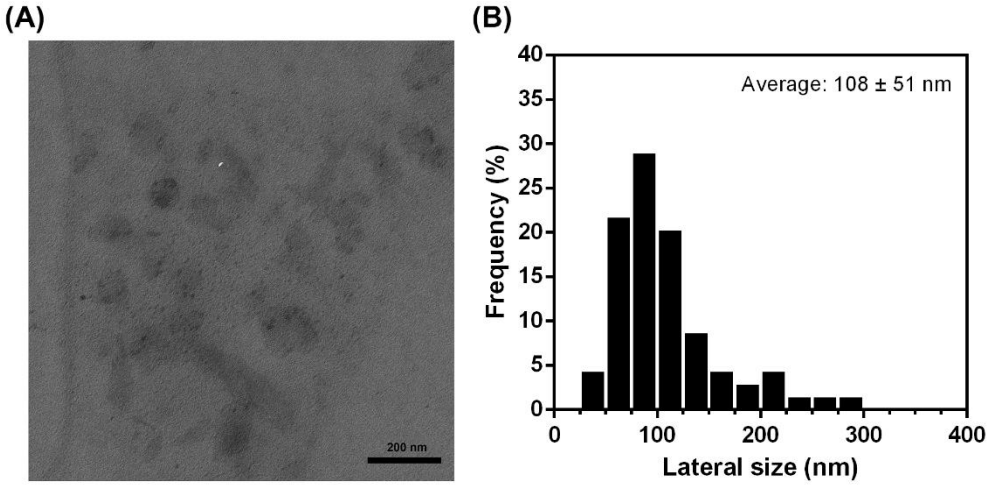

Figure 11: TEM image of HA-rGO (A). Lateral size distribution of HA-rGO determined by measuring the size of HA-rGO based on TEM images (B).

Furthermore, rGO and HA-rGO exhibited a similar NIR absorption, thus confirming that the functionalized rGO preserved its photothermal potential (**Figure 12A**). The direct functionalization of as-prepared rGO with HA-*g*-PMAO led to the production of nanomaterials with suitable physicochemical properties for application in cancer therapy. In contrast, the functionalization of GO reduced by HH usually requires an additional purification step to remove this toxic reducing agent [50, 81]. This fact highlights the convenience of our approach.

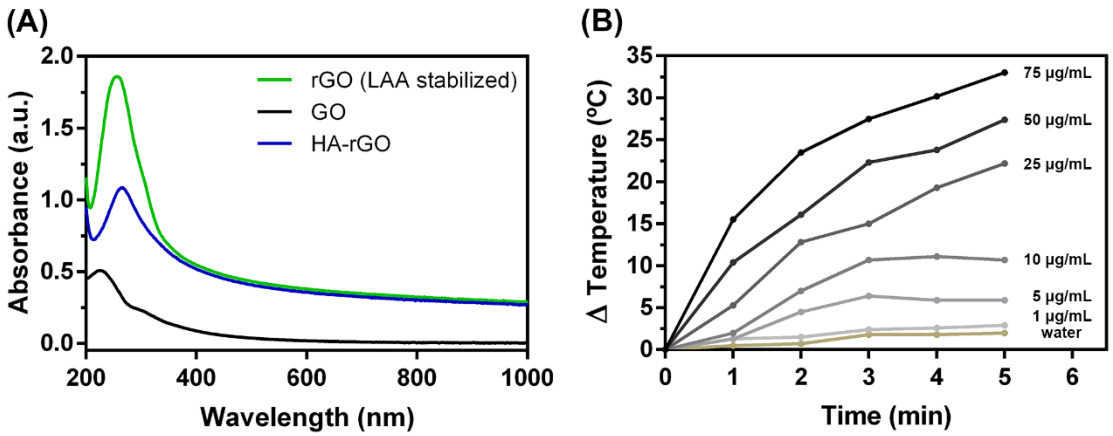

Figure 12: Characterization of the photothermal capacity of HA-rGO. UV-Vis absorption spectra of GO (25 µg/mL), rGO (LAA stabilized; 25 µg/mL of rGO equivalents), and HA-rGO (25 µg/mL of rGO equivalents) (A); Temperature variation curves of HA-rGO at different concentrations (of rGO equivalents) during 5 minutes of NIR irradiation (808 nm, 1.7 W/cm^2) (B).

3.3. Photothermal capacity of HA-rGO

The temperature variations induced, under NIR laser irradiation, by HA-rGO were then studied to confirm the photothermal capacity of this nanomaterial (**Figure 12B**). In general, HA-rGO produced a time and concentration-dependent temperature increase when it was irradiated. After 5 min of irradiation, HA-rGO could induce a temperature increase of about 22 ºC at 25 µg/mL (of rGO equivalents) (**Figure 12B**). In turn, a photoinduced heat of 33 ºC was achieved for the highest concentration tested (75 µg/mL of rGO equivalents) (**Figure 12B**). The attainment of such temperature increase is of paramount importance since it can induce the death of cancer cells [25, 33]. Furthermore, the response of water (control) to NIR light was meaningless (< 2 ºC) (**Figure 12B**). Together, these results confirmed the photothermal efficiency of HA-rGO.

In a previous work, our laboratory developed a hydrothermal treatment (80 ºC for 24 h) to reduce GO and functionalize it with a PEG derivative [38]. When compared to the previous protocol, the HA-rGO preparation method is more convenient since it requires a lower reduction time (1 *vs.* 24 h) [38]. Moreover, HA-rGO also produced a higher photoinduced heat

(33 vs. 27 ºC, at 75 µg/mL of rGO equivalents) [38], thus displaying an enhanced photothermal capacity.

3.4. Cytocompatibility of HA-rGO

Before assessing the phototherapeutic capacity of HA-rGO, the cytocompatibility of this nanomaterial was investigated in MCF-7 cells (breast cancer cell model) and NHDF (healthy cell model). HA-rGO did not induce an acute cytotoxic effect to both cell lines, in the tested concentration range (1-75 µg/mL of rGO equivalents) and incubation times (24 or 48 h) (**Figure 13**). In contrast, rGO (non-functionalized) was showed to induce some cytotoxicity to both cell types (**Figure 14**). In this way, the functionalization of rGO with HA-*g*-PMAO improved its cytocompatibility, which is fundamental for the application of HA-rGO in cancer on-demand therapy.

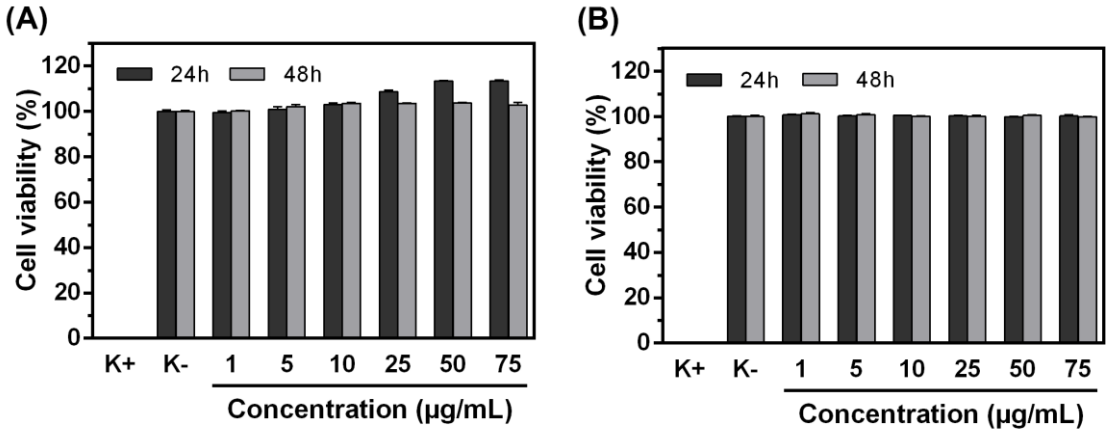

Figure 13: Evaluation of the biocompatibility of HA-rGO. Evaluation of the cytocompatibility of HA-rGO towards MCF-7 cells (A) and NHDF (B) at different concentrations (of rGO equivalents) for 24 and 48h. Data represent mean ± SD, n=5. K- and K+ represent negative and positive controls, respectively.

HA-rGO displayed an enhanced cytocompatibility in comparison to other functionalized rGO materials previously reported in the literature [40, 82]. For instance, PEGylated rGO displayed an IC_{50} towards MCF-7 cells of about 80 µg/mL [40], while HA-rGO did not affect meaningfully the viability of these cells up to 75 µg/mL (of rGO equivalents). In another work, HH-reduced GO functionalized with HA decreased the viability of epidermal carcinoma cells (KB cells) to about 80 % at 40 µg/mL (of rGO equivalents) [82]. Therefore, the environmentally-friendly approach used to reduce GO produces materials with improved cytocompatibility upon functionalization with HA-*g*-PMAO, that may be able to perform a spatial-temporal controlled therapy.

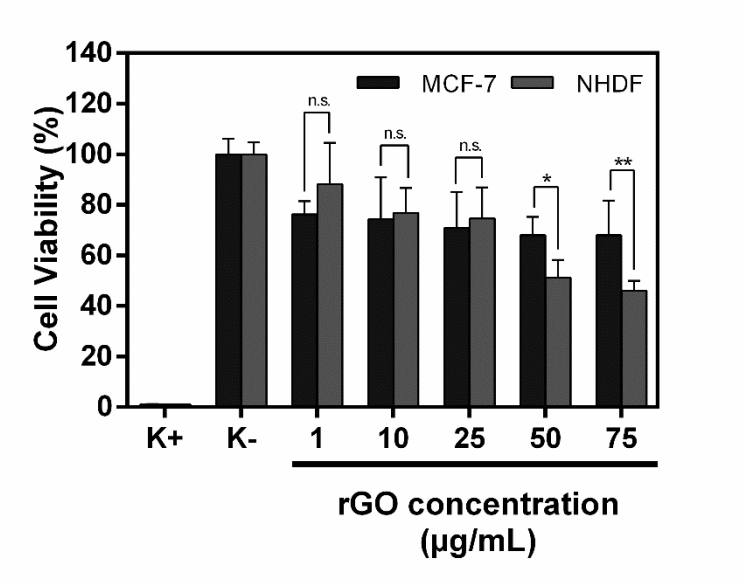

Figure 14: Biocompatibility of rGO at different concentrations towards MCF-7 cells and NHDF after 48 h of incubation. Data represents mean ± SD (*p < 0.05; **p < 0.01), n=5. K+ and K- represent positive and negative controls, respectively. n.s. = non significant

3.5. Targeting capacity of HA-rGO

To confirm the targeting capacity of HA-rGO, the internalization of this nanostructure by MCF-7 cells (CD44 overexpressing cell line) [73, 74] and NHDF (low CD44 expression) [75] was analyzed by CLSM. Prior to this assay, HA-rGO was labelled with Rhod B for its cellular uptake be visualized [47]. The Rhod B labelling was confirmed by analyzing the UV-Vis spectrum of Rhod B labelled HA-rGO (**Figure 15A and 20A**), which displays an absorption peak at 575 nm that is attributed to the fluorescent probe [47].

Moreover, DLS analysis confirmed that the Rhod B labelling did not affect the size distribution of the nanomaterials (**Figure 15B**). Taking into account that rGO based materials have a high fluorescence quenching capacity, we then studied the fluorescence emitted by Rhod B labelled HA-rGO (**Figure 20B**). Compared to free Rhod B, the Rhod B labelled HA-rGO emitted fluorescence with a lower intensity (**Figure 18**). Despite of the quenching effect, the emitted fluorescence signal by Rhod B labelled HA-rGO should still enable its use in CLSM studies [83].

The uptake of Rhod B labelled HA-rGO by MCF-7 cells and NHDF was then studied by CLSM (**Figure 15C**). The results revealed that the internalization profile of the nanostructures by MCF-7 cells and NHDF were different (**Figure 15C**). Fluorescence signals with a higher intensity were observed in the cytoplasm of MCF-7 cells incubated with Rhod B labelled HA-rGO when compared to those found on NHDF (**Figure 15C**). As expected, the internalization of free Rhod B appeared to be similar on both types of cells (**Figure 15C**). In other reports, nanomaterials functionalized with HA also demonstrated a higher uptake by MCF-7 cells [84, 85].

Taken together these results suggest that HA-rGO has a preferential internalization in MCF-7 cells, thus confirming the nanostructures' CD44 targeting ability.

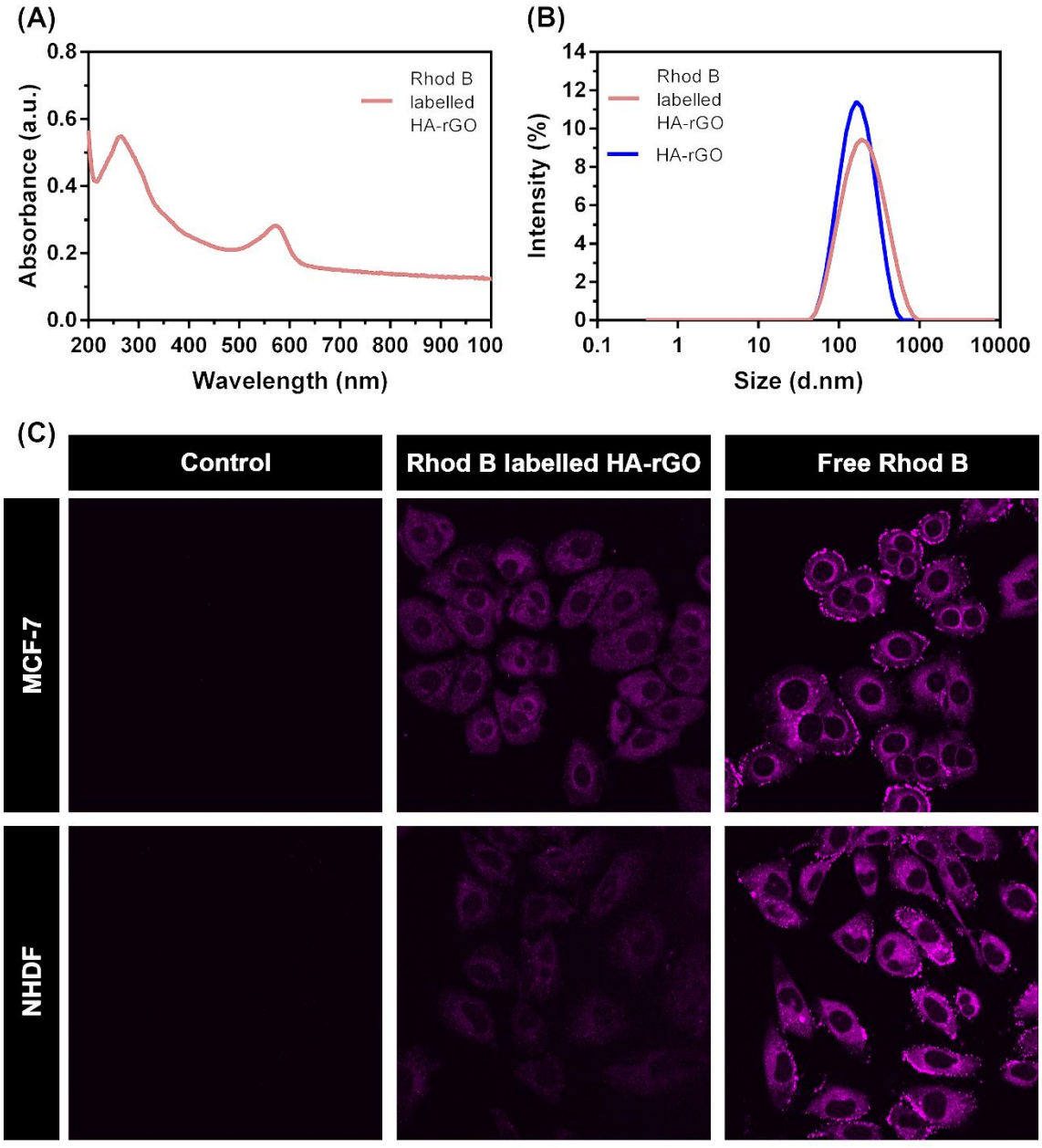

Figure 15: Targeting capacity of HA-rGO. UV-Vis absorption spectra of Rhodamine B labelled HA-rGO (A); DLS size distribution of HA-rGO and Rhod B labelled HA-rGO (B); Representative CLSM images of Rhod B labelled HA-rGO and Free Rhod B uptake by MCF-7 and NHDF cells (C).

3.6. Phototherapeutic effect mediated by HA-rGO

After assessing the HA-rGO cytocompatibility and preferential uptake by MCF-7 cells, the phototherapeutic effect mediated by this nanomaterial was investigated (**Figure 16A**). HA-rGO produced, under NIR laser irradiation, a dose-dependent reduction on MCF-7 cells' viability (**Figure 16B**). At the lowest concentration tested (25 µg/mL of rGO equivalents), HA-rGO did not induce meaningful cytotoxicity towards cancer cells (viability of ≈ 96 %). In stark contrast, the photothermal effect mediated by HA-rGO at 75 µg/mL (of rGO equivalents) induced a reduction of cancer cells' viability to ≈ 6 %. Furthermore, the use of NIR light alone did not induce any toxicity on cancer cells (**Figure 16B**). Additionally, non-irradiated HA-rGO did not induce any deleterious effect on cancer cells (**Figure 16B**). Taken together, these results confirm that HA-rGO can produce an on-demand therapeutic effect upon NIR laser irradiation.

Yu *et al.*, reported that the rGO produced using dopamine as a reducing agent and functionalized with the antiarrhythmic peptide 10 (AAP10) produces a phototherapeutic effect towards MCF-7 cells similar to that of HA-rGO, although it required a higher power density (2 - 2.2 *vs*. 1.7 W/cm^2) and a higher dose (120 *vs*. 75 µg/mL) [86]. In another work, Akhavan and collaborators demonstrated that the PTT mediated by Arginine-glycine-aspartic acid (RGD)-functionalized PEGylated reduced GO nanoribbons induces cancer cells ablation at a low dose (10 µg/mL) but demands a higher intensity (7.5 W/cm^2) and a longer period of irradiation (8 min) [87]. In this way, HA-rGO is a promising nanomaterial to be applied in CD44 targeted cancer PTT.

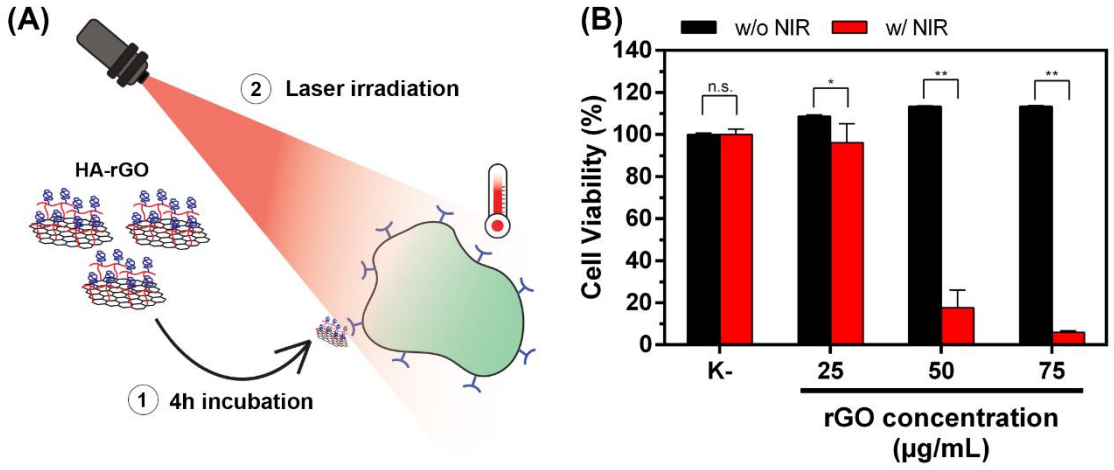

Figure 16: Evaluation of the photothermal capacity of HA-rGO. Schematic representation of the photothermal therapy mediated by HA-rGO (A); Phototherapeutic effect of HA-rGO in MCF-7 cells without NIR (w/o NIR) and with NIR laser irradiation (808 nm, 1.7 W/cm^2, 5 min.) (B). K- w/o NIR represents the negative control. Data represents mean ± SD, n=5 (*p < 0.01; **p < 0.0001), n.s.= non significant.

Chapter 4

Conclusion and Future Perspectives

4. Conclusion and Future Perspectives

Despite all the intensive research on breast cancer, this disease remains as one of the main causes of death in the word. Such is in part due to the sub-optimal efficacy of the currently available treatments (chemotherapy and radiotherapy). Furthermore, these therapeutic approaches also induce severe side effects on patients, thereby contributing for breast cancer mortality.

Researchers have been developing new therapeutic approaches in order to improve breast cancer treatment. In particular, PTT mediated by rGO has been receiving a lot of interest for application in breast cancer treatment. However, this NIR-responsive nanomaterial displays critical limitations (low water solubility, poor colloidal stability, sub-optimal cytocompatibility and non-selectivity towards cancer cells) that hinder its direct use in cancer PTT. The functionalization of rGO with amphiphilic polymers can address the limitations associated to this nanomaterial, except the selectivity problems. Therefore, engineering amphiphilic polymers with targeting capacity is of uttermost importance.

In this dissertation, rGO produced using an environmentally-friendly method was functionalized with a novel HA-based amphiphilic polymer for application in breast cancer PTT. HA was selected due to its hydrophilic character and targeting capacity to the CD44 receptors. The results revealed that treating GO with 3 mM of L-ascorbic acid at 80 ºC during 60 minutes is the optimal green-reducing condition considering the NIR absorption and the size distribution of the produced materials. Then, rGO was functionalized with the HA-based amphiphilic polymer through non-covalent interactions (hydrophobic-hydrophobic interactions). The functionalization of rGO improved its stability, cytocompatibility, and internalization by CD44 overexpressing breast cancer cells, which indicates the targeting capacity of this nanoformulation. Furthermore, the on-demand PTT mediated by HA functionalized rGO induced cancer cells' death.

Overall, the HA functionalized rGO nanomaterials developed in this study are promising platforms for targeted breast cancer therapy. In the future, the encapsulation of chemotherapeutic drugs and imaging agents on the HA functionalized rGO can be explored in order to develop multifunctional theragnostic platforms.

Chapter 5

Bibliographic References

5. Bibliographic References

[1] R.L. Siegel, K.D. Miller, A. Jemal, Cancer statistics, 2018, CA - A Cancer Journal for Clinicians, 68 (2018) 7-30.

[2] www.sns.gov.pt/noticias/2017/04/04/cancro-em-portugal/ (accessed in 29/05/2018).

[3] J.D. Choi, J.S. Lee, Interplay between Epigenetics and Genetics in Cancer, Genomics & informatics, 11 (2013) 164-173.

[4] D. Hanahan, R.A. Weinberg, The hallmarks of cancer, Cell, 100 (2000) 57-70.

[5] Y.A. Fouad, C. Aanei, Revisiting the hallmarks of cancer, American Journal of Cancer Research, 7 (2017) 1016-1036.

[6] D. Hanahan, R.A. Weinberg, Hallmarks of cancer: the next generation, Cell, 144 (2011) 646-674.

[7] E. Witsch, M. Sela, Y. Yarden, Roles for growth factors in cancer progression, Physiology (Bethesda), 25 (2010) 85-101.

[8] E. Chowdhury, S. Tiash, Growth factor receptors: promising drug targets in cancer, Journal of Cancer Metastasis and Treatment, 1 (2015) 190-200.

[9] C.J. Sherr, F. McCormick, The RB and p53 pathways in cancer, Cancer Cell, 2 (2002) 103-112.

[10] R.S. Wong, Apoptosis in cancer: from pathogenesis to treatment, Journal of Experimental & Clinical Cancer Research, 30 (2011) 87.

[11] A. Frenzel, F. Grespi, W. Chmelewskij, A. Villunger, Bcl2 family proteins in carcinogenesis and the treatment of cancer, Apoptosis, 14 (2009) 584-596.

[12] S.E. Artandi, R.A. DePinho, Telomeres and telomerase in cancer, Carcinogenesis, 31 (2010) 9-18.

[13] Z. Wang, C. Dabrosin, X. Yin, M.M. Fuster, A. Arreola, W.K. Rathmell, D. Generali, G.P. Nagaraju, B. El-Rayes, D. Ribatti, Y.C. Chen, K. Honoki, H. Fujii, A.G. Georgakilas, S. Nowsheen, A. Amedei, E. Niccolai, A. Amin, S.S. Ashraf, B. Helferich, X. Yang, G. Guha, D. Bhakta, M.R. Ciriolo, K. Aquilano, S. Chen, D. Halicka, S.I. Mohammed, A.S. Azmi, A. Bilsland, W.N. Keith, L.D. Jensen, Broad targeting of angiogenesis for cancer prevention and therapy, Seminars in Cancer Biology, 35 Suppl (2015) S224-s243.

[14] S. Goel, D.G. Duda, L. Xu, L.L. Munn, Y. Boucher, D. Fukumura, R.K. Jain, Normalization of the vasculature for treatment of cancer and other diseases, Physiol Reviews, 91 (2011) 1071-1121.

[15] K. Polyak, Heterogeneity in breast cancer, Journal of Clinical Investigation, 121 (2011) 3786-3788.

[16] S. Libson, M. Lippman, A review of clinical aspects of breast cancer, International Review of Psychiatry, 26 (2014) 4-15.

[17] www.ligacontracancro.pt/cancro-da-mama (accessed in 29/05/2018).

[18] K. McPherson, C.M. Steel, J.M. Dixon, Breast cancer—epidemiology, risk factors, and genetics, BMJ [British Medical Journal], 321 (2000) 624-628.

[19] K. Polyak, Breast cancer: origins and evolution, Journal of Clinical Investigation, 117 (2007) 3155-3163.

[20] N.R. Bertos, M. Park, Breast cancer - one term, many entities?, Journal of Clinical Investigation, 121 (2011) 3789-3796.

[21] C.E. DeSantis, C.C. Lin, A.B. Mariotto, R.L. Siegel, K.D. Stein, J.L. Kramer, R. Alteri, A.S. Robbins, A. Jemal, Cancer treatment and survivorship statistics, 2014, CA - A Cancer Journal for Clinicians, 64 (2014) 252-271.

[22] C. Twelves, M. Jove, A. Gombos, A. Awada, Cytotoxic chemotherapy: Still the mainstay of clinical practice for all subtypes metastatic breast cancer, Critical Reviews in Oncology/Hematology, 100 (2016) 74-87.

[23] M. Grigore, Organic and Inorganic Nano-systems used in Cancer Treatment, Journal of Medical Research and Health Education, 1 (2017) 1-8.

[24] Y. Tang, Y. Wang, M.F. Kiani, B. Wang, Classification, Treatment Strategy, and Associated Drug Resistance in Breast Cancer, Clinical Breast Cancer, 16 (2016) 335-343.

[25] D. de Melo-Diogo, C. Pais-Silva, D.R. Dias, A.F. Moreira, I.J. Correia, Strategies to Improve Cancer Photothermal Therapy Mediated by Nanomaterials, Advanced Healthcare Materials, 6 (2017).

[26] H. Maeda, Macromolecular therapeutics in cancer treatment: The EPR effect and beyond, Journal of Controlled Release, 164 (2012) 138-144.

[27] S.K. Hobbs, W.L. Monsky, F. Yuan, W.G. Roberts, L. Griffith, V.P. Torchilin, R.K. Jain, Regulation of transport pathways in tumor vessels: Role of tumor type and microenvironment, Proceedings of the National Academy of Sciences, 95 (1998) 4607-4612.

[28] J. Fang, H. Nakamura, H. Maeda, The EPR effect: Unique features of tumor blood vessels for drug delivery, factors involved, and limitations and augmentation of the effect, Advanced Drug Delivery Reviews, 63 (2011) 136-151.

[29] G. Strangman, D.A. Boas, J.P. Sutton, Non-invasive neuroimaging using near-infrared light, Biological Psychiatry, 52 679-693.

[30] T.A. Henderson, L.D. Morries, Near-infrared photonic energy penetration: can infrared phototherapy effectively reach the human brain?, Neuropsychiatric Disease and Treatment, 11 (2015) 2191-2208.

[31] S. Stolik, J.A. Delgado, A. Pérez, L. Anasagasti, Measurement of the penetration depths of red and near infrared light in human “ex vivo” tissues, Journal of Photochemistry and Photobiology B: Biology, 57 (2000) 90-93.

[32] A.M. Smith, M.C. Mancini, S. Nie, Second window for in vivo imaging, Nature Nanotechnology, 4 (2009) 710.

[33] K.F. Chu, D.E. Dupuy, Thermal ablation of tumours: biological mechanisms and advances in therapy, Nature Reviews Cancer, 14 (2014) 199-208.

[34] B.L. Fay, J.R. Melamed, E.S. Day, Nanoshell-mediated photothermal therapy can enhance chemotherapy in inflammatory breast cancer cells, International Journal of Nanomedicine, 10 (2015) 6931-6941.

[35] R.L. Atkinson, M. Zhang, P. Diagaradjane, S. Peddibhotla, A. Contreras, S.G. Hilsenbeck, W.A. Woodward, S. Krishnan, J.C. Chang, J.M. Rosen, Thermal Enhancement with Optically Activated Gold Nanoshells Sensitizes Breast Cancer Stem Cells to Radiation Therapy, Science Translational Medicine, 2 (2010) 55ra79-55ra79.

[36] J.R. Melamed, R.S. Edelstein, E.S. Day, Elucidating the Fundamental Mechanisms of Cell Death Triggered by Photothermal Therapy, ACS Nano, 9 (2015) 6-11.

[37] D. Dias, A. Moreira, I. Correia, The effect of the shape of gold core-mesoporous silica shell nanoparticles on the cellular behavior and tumor spheroid penetration, Journal of Materials Chemistry B, 4 (2016) 7630-7640.

[38] D. de Melo-Diogo, C. Pais-Silva, E.C. Costa, R.O. Louro, I.J. Correia, D-alpha-tocopheryl polyethylene glycol 1000 succinate functionalized nanographene oxide for cancer therapy, Nanomedicine (London, United Kingdom), 12 (2017) 443-456.

[39] M. Hashemi, M. Omidi, B. Muralidharan, H. Smyth, M.A. Mohagheghi, J. Mohammadi, T.E. Milner, Evaluation of the Photothermal Properties of a Reduced Graphene Oxide/Arginine Nanostructure for Near-Infrared Absorption, ACS Applied Materials & Interfaces, 9 (2017) 32607-32620.

[40] J.T. Robinson, S.M. Tabakman, Y. Liang, H. Wang, H. Sanchez Casalongue, D. Vinh, H. Dai, Ultrasmall Reduced Graphene Oxide with High Near-Infrared Absorbance for Photothermal Therapy, Journal of the American Chemical Society, 133 (2011) 6825-6831.

[41] D.R. Dreyer, A.D. Todd, C.W. Bielawski, Harnessing the chemistry of graphene oxide, Chemical Society Reviews, 43 (2014) 5288-5301.

[42] J. Liu, L. Cui, D. Losic, Graphene and graphene oxide as new nanocarriers for drug delivery applications, Acta Biomaterialia, 9 (2013) 9243-9257.

[43] Y. Qiu, F. Guo, R. Hurt, I. Külaots, Explosive thermal reduction of graphene oxide-based materials: Mechanism and safety implications, Carbon, 72 (2014) 215-223.

[44] J.-W. Kim, Y.C. Shin, J.-J. Lee, E.-B. Bae, Y.-C. Jeon, C.-M. Jeong, M.-J. Yun, S.-H. Lee, D.-W. Han, J.-B. Huh, The Effect of Reduced Graphene Oxide-Coated Biphasic Calcium Phosphate Bone Graft Material on Osteogenesis, International Journal of Molecular Sciences, 18 (2017) 1725.

[45] N. Mahanta, A. R. Abramson, Thermal conductivity of graphene and graphene oxide nanoplatelets, in: Thermal and Thermomechanical Phenomena in Electronic Systems (ITherm), IEEE, 2012, pp. 1-6.

[46] M. Orecchioni, R. Cabizza, A. Bianco, L.G. Delogu, Graphene as cancer theranostic tool: progress and future challenges, Theranostics, 5 (2015) 710-723.

[47] L. Zhang, J. Xia, Q. Zhao, L. Liu, Z. Zhang, Functional graphene oxide as a nanocarrier for controlled loading and targeted delivery of mixed anticancer drugs, Small, 6 (2010) 537-544.

[48] S. Pei, H.-M. Cheng, The reduction of graphene oxide, Carbon, 50 (2012) 3210-3228.

[49] X. Gao, J. Jang, S. Nagase, Hydrazine and Thermal Reduction of Graphene Oxide: Reaction Mechanisms, Product Structures, and Reaction Design, Journal of Physical Chemistry C, 114 (2010) 832-842.

[50] K. Yang, J. Wan, S. Zhang, B. Tian, Y. Zhang, Z. Liu, The influence of surface chemistry and size of nanoscale graphene oxide on photothermal therapy of cancer using ultra-low laser power, Biomaterials, 33 (2012) 2206-2214.

[51] H. Kim, D. Lee, J. Kim, T.I. Kim, W.J. Kim, Photothermally triggered cytosolic drug delivery via endosome disruption using a functionalized reduced graphene oxide, ACS Nano, 7 (2013) 6735-6746.

[52] P. Huang, S. Wang, X. Wang, G. Shen, J. Lin, Z. Wang, S. Guo, D. Cui, M. Yang, X. Chen, Surface Functionalization of Chemically Reduced Graphene Oxide for Targeted Photodynamic Therapy, Journal of Biomedical Nanotechnology, 11 (2015) 117-125.

[53] J. Liu, S. Guo, L. Han, T. Wang, W. Hong, Y. Liu, E. Wang, Synthesis of phospholipid monolayer membrane functionalized graphene for drug delivery, Journal of Materials Chemistry, 22 (2012) 20634-20640.

[54] M. Xu, J. Zhu, F. Wang, Y. Xiong, Y. Wu, Q. Wang, J. Weng, Z. Zhang, W. Chen, S. Liu, Improved In Vitro and In Vivo Biocompatibility of Graphene Oxide through Surface Modification: Poly(Acrylic Acid)-Functionalization is Superior to PEGylation, ACS Nano, 10 (2016) 3267-3281.

[55] X. Zhi, H. Fang, C. Bao, G. Shen, J. Zhang, K. Wang, S. Guo, T. Wan, D. Cui, The immunotoxicity of graphene oxides and the effect of PVP-coating, Biomaterials, 34 (2013) 5254-5261.

[56] S.-Y. Wu, S.S.A. An, J. Hulme, Current applications of graphene oxide in nanomedicine, International Journal of Nanomedicine, 10 (2015) 9-24.

[57] Y. Li, L. Feng, X. Shi, X. Wang, Y. Yang, K. Yang, T. Liu, G. Yang, Z. Liu, Surface Coating-Dependent Cytotoxicity and Degradation of Graphene Derivatives: Towards the Design of Non-Toxic, Degradable Nano-Graphene, Small, 10 (2014) 1544-1554.

[58] L. Chen, X. Zhong, X. Yi, M. Huang, P. Ning, T. Liu, C. Ge, Z. Chai, Z. Liu, K. Yang, Radionuclide 131I labeled reduced graphene oxide for nuclear imaging guided combined radio- and photothermal therapy of cancer, Biomaterials, 66 (2015) 21-28.

[59] A. Yuan, X. Qiu, X. Tang, W. Liu, J. Wu, Y. Hu, Self-assembled PEG-IR-780-C13 micelle as a targeting, safe and highly-effective photothermal agent for in vivo imaging and cancer therapy, Biomaterials, 51 (2015) 184-193.

[60] J.V. Jokerst, T. Lobovkina, R.N. Zare, S.S. Gambhir, Nanoparticle PEGylation for imaging and therapy, Nanomedicine (London, United Kingdom), 6 (2011) 715-728.

[61] A. Omid, G. Elham, Graphene Nanomesh Promises Extremely Efficient In Vivo Photothermal Therapy, Small, 9 (2013) 3593-3601.

[62] Y. Wang, Y. Lei, J. Li, L. Gu, H. Yuan, D. Xiao, Synthesis of 3D-Nanonet Hollow Structured Co3O4 for High Capacity Supercapacitor, ACS Applied Materials & Interfaces, 6 (2014) 6739-6747.

[63] X. Yang, J.J. Grailer, I.J. Rowland, A. Javadi, S.A. Hurley, V.Z. Matson, D.A. Steeber, S. Gong, Multifunctional stable and pH-responsive polymer vesicles formed by heterofunctional triblock copolymer for targeted anticancer drug delivery and ultrasensitive MR imaging, ACS Nano, 4 (2010) 6805-6817.

[64] X. Hu, X. Jing, Biodegradable amphiphilic polymer–drug conjugate micelles, Expert Opinion on Drug Delivery, 6 (2009) 1079-1090.

[65] L.C. Becker, W.F. Bergfeld, D.V. Belsito, C.D. Klaassen, J.G. Marks, Jr., R.C. Shank, T.J. Slaga, P.W. Snyder, F.A. Andersen, Final report of the safety assessment of hyaluronic acid, potassium hyaluronate, and sodium hyaluronate, International Journal of Toxicology, 28 (2009) 5-67.

[66] G. Mattheolabakis, L. Milane, A. Singh, M.M. Amiji, Hyaluronic acid targeting of CD44 for cancer therapy: from receptor biology to nanomedicine, Journal of Drug Targeting, 23 (2015) 605-618.

[67] C. Yang, Y. He, H. Zhang, Y. Liu, W. Wang, Y. Du, F. Gao, Selective killing of breast cancer cells expressing activated CD44 using CD44 ligand-coated nanoparticles in vitro and in vivo, Oncotarget, 6 (2015) 15283-15296.

[68] S. Misra, V.C. Hascall, R.R. Markwald, S. Ghatak, Interactions between Hyaluronan and Its Receptors (CD44, RHAMM) Regulate the Activities of Inflammation and Cancer, Frontiers in Immunology, 6 (2015) 201.

[69] S. Hiscox, B. Baruha, C. Smith, R. Bellerby, L. Goddard, N. Jordan, Z. Poghosyan, R.I. Nicholson, P. Barrett-Lee, J. Gee, Overexpression of CD44 accompanies acquired tamoxifen resistance in MCF7 cells and augments their sensitivity to the stromal factors, heregulin and hyaluronan, BMC Cancer, 12 (2012) 458.

[70] K. Yang, L. Feng, H. Hong, W. Cai, Z. Liu, Preparation and functionalization of graphene nanocomposites for biomedical applications, Nature Protocols, 8 (2013).

[71] M.J. Fernández-Merino, L. Guardia, J.I. Paredes, S. Villar-Rodil, P. Solís-Fernández, A. Martínez-Alonso, J.M.D. Tascón, Vitamin C Is an Ideal Substitute for Hydrazine in the Reduction of Graphene Oxide Suspensions, Journal of Physical Chemistry C, 114 (2010) 6426-6432.

[72] V.M. Gaspar, P. Baril, E.C. Costa, D. de Melo-Diogo, F. Foucher, J.A. Queiroz, F. Sousa, C. Pichon, I.J. Correia, Bioreducible poly(2-ethyl-2-oxazoline)-PLA-PEI-SS triblock copolymer

micelles for co-delivery of DNA minicircles and Doxorubicin, Journal of Controlled Release, 213 (2015) 175-191.

[73] A.M. Calcagno, C.D. Salcido, J.-P. Gillet, C.-P. Wu, J.M. Fostel, M.D. Mumau, M.M. Gottesman, L. Varticovski, S.V. Ambudkar, Prolonged Drug Selection of Breast Cancer Cells and Enrichment of Cancer Stem Cell Characteristics, JNCI, Journal of the National Cancer Institute, 102 (2010) 1637-1652.

[74] E. Olsson, G. Honeth, P.-O. Bendahl, L.H. Saal, S. Gruvberger-Saal, M. Ringnér, J. Vallon-Christersson, G. Jönsson, K. Holm, K. Lövgren, M. Fernö, D. Grabau, Å. Borg, C. Hegardt, CD44 isoforms are heterogeneously expressed in breast cancer and correlate with tumor subtypes and cancer stem cell markers, BMC Cancer, 11 (2011) 418.

[75] Y. Miyatake, A.L. Oliveira, M.A. Jarboui, S. Ota, U. Tomaru, T. Teshima, W.W. Hall, M. Kasahara, Protective roles of epithelial cells in the survival of adult T-cell leukemia/lymphoma cells, American Journal of Pathology, 182 (2013) 1832-1842.

[76] S.M. Hussain, J.M. Frazier, Cellular Toxicity of Hydrazine in Primary Rat Hepatocytes, Toxicological Sciences, 69 (2002) 424-432.

[77] J. Zhang, H. Yang, G. Shen, P. Cheng, J. Zhang, S. Guo, Reduction of graphene oxide vial-ascorbic acid, Chemical Communications, 46 (2010) 1112-1114.

[78] M. He, Z. Zhao, L. Yin, C. Tang, C. Yin, Hyaluronic acid coated poly(butyl cyanoacrylate) nanoparticles as anticancer drug carriers, International Journal of Pharmaceutics, 373 (2009) 165-173.

[79] J. Huang, H. Zhang, Y. Yu, Y. Chen, D. Wang, G. Zhang, G. Zhou, J. Liu, Z. Sun, D. Sun, Y. Lu, Y. Zhong, Biodegradable self-assembled nanoparticles of poly (D-L-lactide-co-glycolide)/hyaluronic acid block copolymers for target delivery of docetaxel to breast cancer, Biomaterials, 35 (2014) 550-566.

[80] J. Li, M. Huo, J. Wang, J. Zhou, J.M. Mohammad, Y. Zhang, Q. Zhu, A.Y. Waddad, Q. Zhang, Redox-sensitive micelles self-assembled from amphiphilic hyaluronic acid-deoxycholic acid conjugates for targeted intracellular delivery of paclitaxel, Biomaterials, 33 (2012) 2310-2320.

[81] H.P. Mungse, O.P. Khatri, Chemically Functionalized Reduced Graphene Oxide as a Novel Material for Reduction of Friction and Wear, Journal of Physical Chemistry C, 118 (2014) 14394-14402.

[82] W. Miao, G. Shim, C.M. Kang, S. Lee, Y.S. Choe, H.-G. Choi, Y.-K. Oh, Cholesteryl hyaluronic acid-coated, reduced graphene oxide nanosheets for anti-cancer drug delivery, Biomaterials, 34 (2013) 9638-9647.

[83] Y. Zhong, K. Goltsche, L. Cheng, F. Xie, F. Meng, C. Deng, Z. Zhong, R. Haag, Hyaluronic acid-shelled acid-activatable paclitaxel prodrug micelles effectively target and treat CD44-overexpressing human breast tumor xenografts in vivo, Biomaterials, 84 (2016) 250-261.

[84] X. Gao, J. Zhang, Q. Xu, Z. Huang, Y. Wang, Q. Shen, Hyaluronic acid-coated cationic nanostructured lipid carriers for oral vincristine sulfate delivery, Drug Development and Industrial Pharmacy, 43 (2017) 661-667.

[85] J. Wang, W. Ma, Q. Guo, Y. Li, Z. Hu, Z. Zhu, X. Wang, Y. Zhao, X. Chai, P. Tu, The effect of dual-functional hyaluronic acid-vitamin E succinate micelles on targeting delivery of doxorubicin, International Journal of Nanomedicine, 11 (2016) 5851-5870.

[86] J. Yu, Y.H. Lin, L. Yang, C.C. Huang, L. Chen, W.C. Wang, G.W. Chen, J. Yan, S. Sawettanun, C.H. Lin, Improved Anticancer Photothermal Therapy Using the Bystander Effect Enhanced by Antiarrhythmic Peptide Conjugated Dopamine-Modified Reduced Graphene Oxide Nanocomposite, Advanced Healthcare Materials, 6 (2017) 1600804.

[87] O. Akhavan, E. Ghaderi, S. Aghayee, Y. Fereydooni, A. Talebi, The use of a glucose-reduced graphene oxide suspension for photothermal cancer therapy, Journal of Materials Chemistry, 22 (2012) 13773-13781.

[88] T. Wada, S. Chirachanchai, N. Izawa, Y. Inaki, K. Takemoto, Synthesis and Properties of Hyaluronic Acid Conjugated Nucleic Acid Analogs—1: Synthesis of Deacetylhyaluronan and Introduction of Nucleic Acid Bases, Journal of Bioactive and Compatible Polymers, 9 (1994) 429-447.

[89] S.M. Henry, M.E.H. El-Sayed, C.M. Pirie, A.S. Hoffman, P.S. Stayton, pH-Responsive Poly(styrene-alt-maleic anhydride) Alkylamide Copolymers for Intracellular Drug Delivery, Biomacromolecules, 7 (2006) 2407-2414.

[90] J. Qiu, R. Cheng, J. Zhang, H. Sun, C. Deng, F. Meng, Z. Zhong, Glutathione-Sensitive Hyaluronic Acid-Mercaptopurine Prodrug Linked via Carbonyl Vinyl Sulfide: A Robust and CD44-Targeted Nanomedicine for Leukemia, Biomacromolecules, 18 (2017) 3207-3214.

Chapter 6

Appendix

6. Appendix

6.1. Deacetylation of Hyaluronic acid

Deacetylated Hyaluronic Acid (dHA) was prepared following a method described elsewhere with slight modifications [88]. Briefly, 250 mg of HA)were dissolved in 12.5 mL of NaOH 13.7N. This solution was left to stir for 2 h at 60 ºC. Afterward, the solution's pH was adjusted to 7 with HCl 5N. The resulting solution was dialyzed against water (3.5 kDa cut-off dialysis membrane) for 3 days and it was then freeze-dried (ScanVac CoolSafe, LaboGene Aps, Lynge, Denmark), yielding deacetylated HA.

Previous to the deacetylation, the FTIR spectrum of HA exhibited a small peak at 1737 cm^{-1} (C=O stretch), that can be attributed to ketone groups (**Figure 17**). The intensity of this peak decreased after deacetylation, thus demonstrating the successful of production of dHA **(Figure 17**).

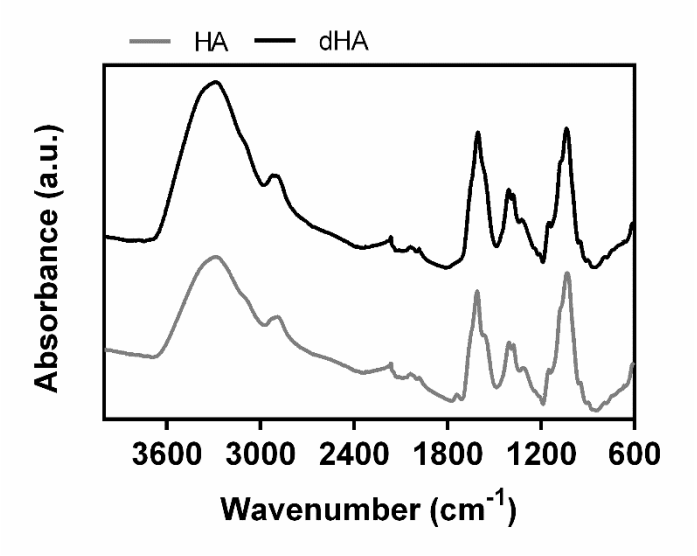

Figure 17: FTIR spectra of HA and dHA.

6.2. Opening of the Anhydride ring of PMAO

Hydrolyzed PMAO (oPMAO) was produced by adapting a method previously described in the literature [89]. In brief, 4 mL of a solution of NaOH 2N was added to 200 mg of PMAO and allowed to stir for 5 h at room temperature (RT). After adjusting the pH to 7, the opaque solution was dialyzed against water (14kDa cut-off dialysis membrane) for 1 day and then was freeze-dried, yielding oPMAO.

Previous to the hydrolysis, the FTIR spectrum of PMAO displayed peaks at 1856 cm^{-1} and 1776 cm^{-1} (C=O stretches), which are characteristic of the anhydride ring. After the base-catalyzed hydrolysis of PMAO, the previous peaks disappeared. Furthermore, the FTIR spectrum of oPMAO displayed new peaks at 1698 cm^{-1} and 1558 cm^{-1} (C=O stretches), which can be attributed to carboxylic acid groups, thereby confirming the opening of the PMAO anhydride rings (**Figure 18**).

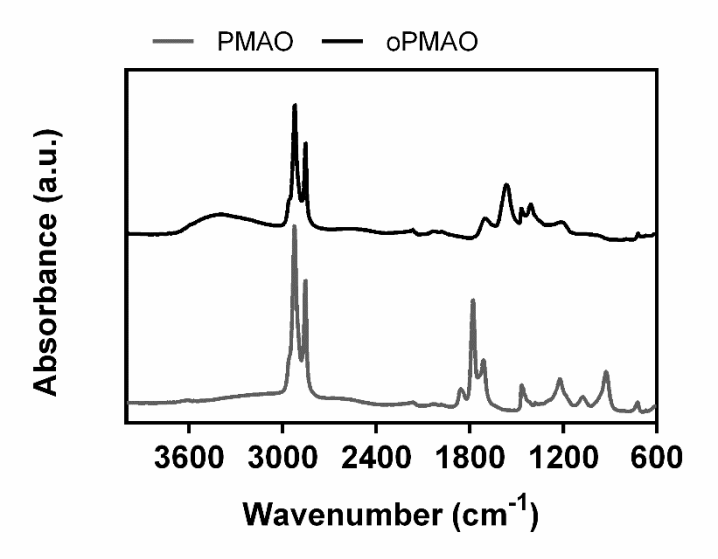

Figure 18: FTIR spectra of PMAO and oPMAO.

6.3. Preparation of HA grafted PMAO

To obtain HA-grafted PMAO (HA-*g*-PMAO), oPMAO was conjugated with dHA through EDC chemistry [90]. In brief, 50 mg of oPMAO was activated with EDC (27.3 mg) and NHS (16.4 mg) for 1 h (RT) in 25 mL of DMSO. Afterward, 50 mg of dHA dissolved in water was added dropwise to the former solution. This solution was allowed to stir for another 5 h, at RT. Then, the solution was dialyzed against water (14 kDa cut-off dialysis membrane) and it was freeze-dried, yielding HA-*g*-PMAO.

HA-*g*-PMAO FTIR spectrum displayed peaks at 2919 and 2850 cm^{-1} (C-H stretch), which are also present in the spectrum of oPMAO. Furthermore, a peak at 1043 cm^{-1} (primary alcohol C-O stretch) is also present on the FTIR spectra of dHA and HA-*g*-PMAO (**Figure 19**). The spectrum of HA-*g*-PMAO displays a peak at 1639 cm^{-1} (secondary amide stretch), which confirm the conjugation of the primary amines of dHA with the carboxylic acid groups of oPMAO (**Figure 19**). Taken together these results confirm the successful preparation of HA-*g*-PMAO.

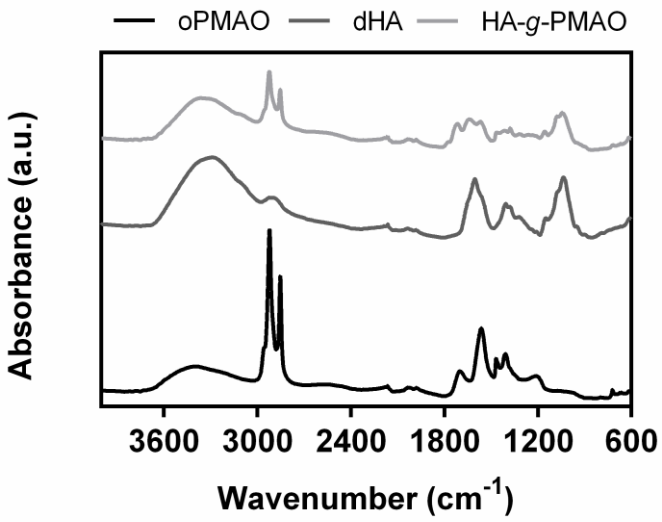

Figure 19: FTIR spectra of oPMAO, dHA, and HA-*g*-PMAO.

6.4. Characterization of Rhodamine B labelled HA-rGO

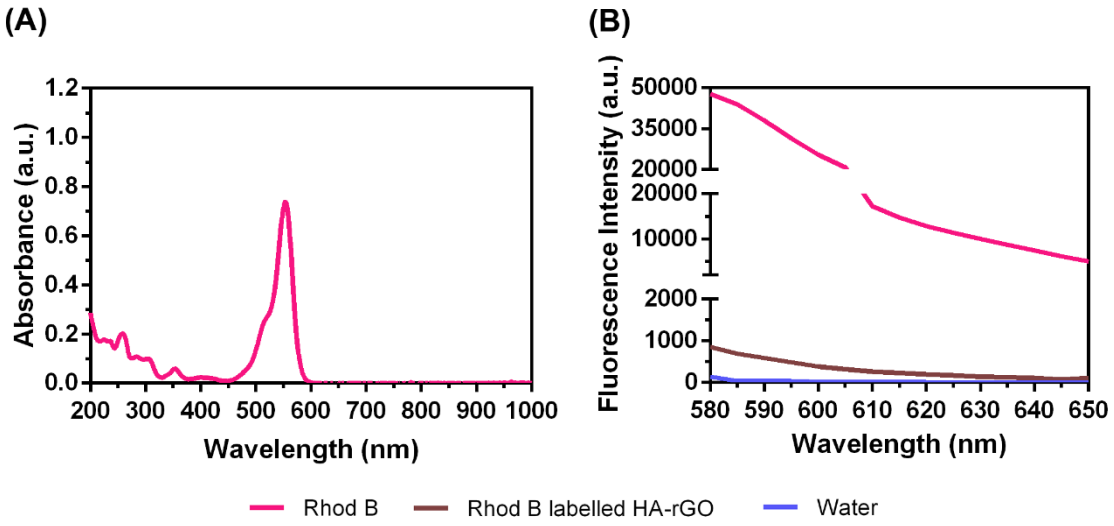

Figure 20: UV-Vis absorption and fluorescence spectra of Rhodamine B and Rhodamine B-labelled HA-rGO. UV-Vis absorption spectra of free Rhodamine B (dissolved in water) (A); Fluorescence spectra of free Rhod B, Rhod B labelled HA-rGO and water (excitation at 560 nm) (B).